LA-UR-17-30646 (Accepted Manuscript)

Intracellular Hepatitis C Virus Modeling Predicts Infection Dynamics and Viral Protein Mechanisms

Aunins, Thomas R.
Marsh, Katherine M.
Uprichard, Susan L.
Perelson, Alan S.
Chatterjee, Anushree

Provided by the author(s) and the Los Alamos National Laboratory (2018-07-03).

To be published in: Journal of Virology

DOI to publisher's version: 10.1128/JVI.02098-17

Permalink to record: http://permalink.lanl.gov/object/view?what=info:lanl-repo/lareport/LA-UR-17-30646

Disclaimer:
Approved for public release. Los Alamos National Laboratory, an affirmative action/equal opportunity employer, is operated by the Los Alamos National Security, LLC for the National Nuclear Security Administration of the U.S. Department of Energy under contract DE-AC52-06NA25396. Los Alamos National Laboratory strongly supports academic freedom and a researcher's right to publish; as an institution, however, the Laboratory does not endorse the viewpoint of a publication or guarantee its technical correctness.

JVI Accepted Manuscript Posted Online 21 March 2018
J. Virol. doi:10.1128/JVI.02098-17
Copyright © 2018 American Society for Microbiology. All Rights Reserved.

Accepted Manuscript Posted Online

Journal of Virology

JVI

Journal of Virology

Downloaded from http://jvi.asm.org/ on March 26, 2018 by LANL Research Library

Intracellular hepatitis C modeling predicts infection dynamics and viral protein mechanisms

Thomas R. Aunins[a], Katherine A. Marsh[b], Gitanjali Subramanya[c], Susan L. Uprichard[b,c], Alan S. Perelson[d], and Anushree Chatterjee[a,e#]

[a]Department of Chemical and Biological Engineering, University of Colorado Boulder

[b]Department of Microbiology and Immunology, University of Illinois Chicago, Chicago, IL, USA.

[c]Program for Experimental & Theoretical Modeling, Division of Hepatology, Department of Medicine, Loyola University Medical Center, Maywood, IL, USA.

[d]Theoretical Biology and Biophysics Group, Los Alamos National Laboratory, NM, USA.

[e]BioFrontiers Institute, University of Colorado Boulder

Running Title: Hepatitis C intracellular infection model

#Address correspondence to Anushree Chatterjee, chatterjee@colorado.edu

Abstract word count: 231

Manuscript word count: 8039

Accepted Manuscript Posted Online

Journal of Virology

JVI

Journal of Virology

Downloaded from http://jvi.asm.org/ on March 26, 2018 by LANL Research Library

Abstract

Hepatitis C virus infection is a global health problem, with nearly 2 million new infections occurring every year and up to 85% of these becoming chronic infections that pose serious long-term health risks. To effectively reduce the prevalence of HCV infection and associated diseases, it is important to understand the intracellular dynamics of the viral lifecycle. Here, we present a detailed mathematical model that represents the full hepatitis C lifecycle. It is the first full HCV model to be fit to acute intracellular infection data and the first to explore the functions of distinct viral proteins, probing multiple hypotheses of *cis*- and *trans*-acting mechanisms to provide insights for drug targeting. Model parameters were derived from the literature, experiments, and fitting to experimental intracellular viral RNA, extracellular viral titer, and HCV core and NS3 protein kinetic data from viral inoculation to steady-state. Our model predicts faster rates for protein translation and polyprotein cleavage than previous replicon models and demonstrates that the processes of translation and synthesis of viral RNA have the most influence on the levels of the species we tracked in experiments. Overall, our experimental data and the resulting mathematical infection model reveal information about the regulation of core protein during infection, produce specific insights into the roles of the viral core, NS5A, and NS5B proteins, and demonstrate the sensitivities of viral proteins and RNA to distinct reactions within the lifecycle.

Keywords: Hepatitis C virus, mathematical model, polyprotein cleavage, RNA

Accepted Manuscript Posted Online

Journal of Virology

JVI

Journal of Virology

Downloaded from http://jvi.asm.org/ on March 26, 2018 by LANL Research Library

Importance

We have designed a model for the full lifecycle of hepatitis C virus. Past efforts have largely focused on modeling hepatitis C replicon systems, in which transfected subgenomic HCV RNA maintains autonomous replication in the absence of virion production or spread. We started with the general structure of these previous replicon models and expanded to create a model that incorporates the full virus lifecycle as well as additional intracellular mechanistic detail. We compared several different hypotheses that have been proposed for different parts of the lifecycle and applied the corresponding model variations to infection data to determine which hypotheses are most consistent with the empirical kinetic data. Because the infection data we have collected for this study is a more physiologically relevant representation of a viral lifecycle than data obtained from a replicon system, our model can make more accurate predictions about clinical hepatitis C infections.

Accepted Manuscript Posted Online

Journal of Virology

JVI

Journal of Virology

Downloaded from http://jvi.asm.org/ on March 26, 2018 by LANL Research Library

Introduction

Hepatitis C virus (HCV) is one of the most prevalent viruses in the world, with an estimated 71 million people worldwide affected by chronic infection (1). Despite the existence of effective direct-acting antiviral treatments, which can effectively cure more than 90% of HCV cases treated, many people infected with the virus do not have access to these expensive drugs and remain untreated (2–4). It is estimated that approximately 399,000 people die every year due to cirrhosis or hepatocellular carcinoma associated with current or past chronic HCV infection (1). Further study of the virus will help to yield greater understanding of the viral lifecycle, which could help to expand treatment options, target resistant strains, and/or limit HCV-associated pathology.

HCV is a blood-borne plus-stranded RNA virus of the family *Flaviviridae* that infects hepatocytes and maintains virion production over the course of years, sustaining a chronic infection which often results in minimal symptoms for much of this period (5). The viral particle consists of an enveloped capsid containing an approximately 9,600 nucleotide genomic RNA. The HCV life cycle begins with endocytosis of a viral particle into the host cell and the subsequent uncoating and release of the viral RNA into the cytoplasm. This viral genome serves as template for host cell ribosomes to translate the virally encoded polyprotein, which is subsequently cleaved into individual viral proteins by a combination of both viral and host proteases (Figure 1A). Once synthesized, the viral non-structural proteins remodel the host cell membranes to form viral replication compartments referred to as the vesicular membranous structure (VMS). Here the viral polymerase, in concert with other non-structural proteins, amplifies the viral genomic RNA through a negative-strand intermediate. Newly synthesized viral RNA is then either utilized to translate more viral proteins or packaged into capsids made

Accepted Manuscript Posted Online

Journal of Virology

JVI

up of the core protein. These RNA-containing capsids are enveloped as they bud into the endoplasmic reticulum, picking up the viral envelope glycoproteins E1 and E2, and are secreted from the cell via the secretory pathway.

Development of the HCV subgenomic replicon model in 1999 demonstrated that 5 of the non-structural proteins (NS3, NS4A, NS4B, NS5A and NS5B) are necessary and sufficient for HCV RNA replication (6). While subgenomic replicons do not recapitulate the full viral lifecycle, they provide a useful experimental system for studying HCV replication dynamics. Two notable HCV subgenomic replicon mathematical models have been developed in the past decade: the first one built in 2007 by Dahari et al. which was fit to steady-state HCV replicon data (7), and another in 2013 by Binder et al. which expanded upon that model to capture the early dynamics of the HCV replicon system immediately post-transfection of subgenomic RNA into host cells (8). The primary difference between the two models is the import step of RNA into the VMS, a reaction which was updated in the later model to incorporate an interaction with a limited quantity of a host factor molecule and to represent the *cis*-acting behavior of the viral RNA polymerase NS5B. This behavior has been described in HCV as well as other flaviviruses and RNA viruses (9–11). The structure of the Binder model has also been integrated into a multi-scale infection model by Clausznitzer et al. to study patient-to-patient variation in response to treatment with the NS5A inhibitor daclatasvir (12). The Clausznitzer model added virus entry and egress processes, as well as a generalized structural protein involved in viral particle assembly and egress. However, most parameters in the multi-scale model were taken from the Binder model and new reaction constants were fit only to extracellular viral load data, which makes it difficult to draw direct conclusions about intracellular processes during infection.

Downloaded from http://jvi.asm.org/ on March 26, 2018 by LANL Research Library

Journal of Virology

Accepted Manuscript Posted Online

Journal of Virology

JVI

Journal of Virology

Downloaded from http://jvi.asm.org/ on March 26, 2018 by LANL Research Library

Our efforts began with an evaluation of the structures used in these models to determine where more detail or improvements could be made. The previous models lump viral proteins into a single entity, making it impossible to separate individual functions. Furthermore, the assumed *cis*-acting behavior of the viral polymerase (NS5B) as well as other viral NS proteins in the previous models limited how the activity of these proteins could be represented. We address these issues by incorporating more detail across the replication cycle and focusing on distinctions between HCV non-structural proteins. In addition, we have expanded upon these replicon models to include viral infection initiation and secretion of progeny HCV particles from the host cell, and have incorporated new experimental data about protein degradation rates to create a detailed mathematical model of HCV infection *in vitro*. We then trained and validated this model by fitting to experimental RNA and protein data produced using the JFH-1 HCV cell culture (HCVcc) system. Here, we present this comprehensive model and use it to probe individual viral protein *cis*- and *trans*-acting functions, protein regulation, and assess the function of the VMS.

Accepted Manuscript Posted Online

Journal of Virology

JVI

Journal of Virology

Downloaded from http://jvi.asm.org/ on March 26, 2018 by LANL Research Library

Results

The Hepatitis C Infection Model

Our infection model was developed by expanding and modifying the basic structure of previous models to accommodate observations from the experimental literature and our own experimental data. The final model schematic is shown in Figure 1B. This model consists of 21 biological reactions with 15 reaction constants (Table 1) and 17 species that yield 17 differential equations to represent their time-dependent concentrations (See Methods).

To represent a single virus initiating infection, there is one plus-stranded RNA molecule at the start of the simulation at 0 hours. In Step 1 of the model, the cytoplasmic HCV RNA associates with available ribosomes in a second order reaction to form a translation complex (TC) at a rate k_{TC}. This complex then synthesizes the viral polyprotein in a first order reaction with rate constant $k_{translation}$. In Step 2, the viral structural proteins (generalized as S), and the nonstructural proteins (with NS3/4A, NS5A, and NS5B specifically represented in the model) are cleaved simultaneously to represent the rapid processing of the viral polyprotein that has been reported in the literature (13, 14). In Step 3, we assume that a single cytoplasmic HCV RNA and NS5B associate to form a 1:1 RNA/NS5B complex at rate k_{Rp5B}, and a free host factor (HF) associates with NS5A to form a HF/NS5A complex at rate k_{HFC}, both in second order reactions according to the reactant concentrations. These two complexes are then imported into the VMS in a second order reaction at rate k_{Rip} to produce a R_{ip} (**R**NA **p**lus-stranded **i**ntermediate) complex that will make minus-strand RNA. In Step 4, inside the VMS, the minus-strand is synthesized—creating a double-strand molecule (dsRNA)—in a first order reaction with rate constant $k_{inititation}$. Next, in Step 5, the dsRNA molecule associates with NS5B to form the R_{ids} (**R**NA **d**ouble-**s**tranded

Accepted Manuscript Posted Online

Journal of Virology

JVI

Journal of Virology

Downloaded from http://jvi.asm.org/ on March 26, 2018 by LANL Research Library

intermediate) complex, a second order reaction at rate k_{Rids}, which then synthesizes new plus-strand RNA in a first order reaction with rate constant $k_{replication}$. This double-stranded molecule remains in the VMS to continue synthesizing plus-strand RNA. New plus-stranded RNA in the VMS can be exported into the cytoplasm in a first order reaction at rate k_{outRp} for subsequent translation of viral proteins or, in Step 6, be assembled into a virus particle and exported from the cell through association with cytoplasmic structural protein, a second order reaction at rate $k_{assembly}$ (Figure 1B; Table 1 and 2). This model was finalized after a comparison of several hypothesized mechanisms to find the one able to best fit our experimental data. These variant models were constructed and evaluated to address the main goals of our system as follows:

Roles of *cis*- and *trans*-acting viral proteins. A key element of the most recent replicon model's structure is the direct import of translation complexes into the VMS in a third order reaction with a cellular host factor molecule and a single viral protein. This was meant to recapitulate the proximity of the viral RNA to protein translated from it, as well as the *cis*-acting behavior of the non-structural proteins, most of which at the time had yet to be found capable of being *trans*-complemented (8). However, with more recent data indicating the ability for *trans*-complementation of the HCV non-structural proteins (15), one goal of our model was to examine and probe this concept further, and to more accurately portray the *cis*-/*trans*-acting behavior of the HCV nonstructural proteins involved in replication (NS3-NS5B).

Individually, the protein NS3 is acknowledged to assist in several processes throughout the viral lifecycle (16, 17), but its most essential and well-defined function is performed in tandem with the cofactor NS4A as a critical viral protease. Therefore, our model treats these two proteins as a single unit, acting only in their protease function and cleaving themselves and the downstream viral proteins from the HCV polyprotein (18). The protease activity of NS3/4A only functions

Accepted Manuscript Posted Online

Journal of Virology

JVI

Journal of Virology

Downloaded from http://jvi.asm.org/ on March 26, 2018 by LANL Research Library

in *cis* (10, 15), and for this reason the subsequent cleavage steps were chosen to be first order reactions, with the activity of NS3/4A encompassed in the reaction constants, as the whole-cell concentration of this protein will not affect the rate of *cis*-acting activity.

The viral protein NS4B, like its neighbors in the polyprotein, takes part in a number of viral functions, but its most distinct role is in helping to assemble the membranous web architecture of the VMS (19, 20). The functional role of NS4B was not included in the model because the sequence and process of VMS formation remain largely unknown and likely involve many host molecules as well as NS4B self-interaction (21), which would add complexity without adequate mechanistic understanding or justification.

Research in the past decade has consistently demonstrated the potential for the viral protein NS5A to be *trans*-complemented when deactivating mutations are introduced into the replicon NS5A sequence (10, 15). Previous models have used a single generalized non-structural protein, and allowed the cytoplasmic role of that protein to be supplied in *trans*, ostensibly representing the function of the protein NS5A. However, once inside the VMS, the generalized non-structural protein in these models switches to acting like the viral RNA polymerase NS5B (7, 8, 12). Our model was designed to separate these functions to better assess the individual importance and sensitivity of the system to NS5A and NS5B individually.

The NS5A protein has been implicated in a diverse and complex set of viral processes within the cell, with different domains of the protein associated viral replication and viral particle assembly (16, 22–25). The various functions of this protein appear to be modulated by phosphorylation state and binding to an array of cellular host factors, including the host factor cyclophilin A, and these interactions have been explored as a target of HCV treatment (26–31).

Accepted Manuscript Posted Online

Journal of Virology

JVI

Journal of Virology

Downloaded from http://jvi.asm.org/ on March 26, 2018 by LANL Research Library

To incorporate NS5A individually in our model, we assume that after cleavage from the polyprotein NS5A associates with a generalized host factor to form a host factor complex. This is meant to encompass the various interactions between NS5A and the host environment. Following this step, the NS5A-host factor complex associates with a complex which includes NS5B and HCV plus-stranded RNA to create a replication complex, which is imported into the VMS (Figure 1B, Step 4). This is consistent with activity of cyclophilin A, which associates with both NS5A and NS5B, and localizes to the VMS during HCV replication (32). It also agrees with prior research that has shown that NS5A is required for the formation of double-membraned vesicles within the VMS, which house the HCV replication complexes (33). Finally, it is consistent with studies that have shown that NS5A exhibits RNA-binding activity required for the initiation of replication (34, 35). To simplify our model, the viral particle assembly function of NS5A (36, 37) was omitted, though this mechanism may be of interest in future investigations.

The RNA-dependent RNA polymerase NS5B is critical for a productive hepatitis C infection and is an important therapeutic target (22), which makes its role in the viral lifecycle important to understand. The primary role of NS5B is in the synthesis of minus and plus-strand viral RNA within the VMS (16), which is also the primary role it holds within this model. Despite prior belief that NS5B must function in *cis*, recent *trans*-complementation studies show that in a system where the polymerase function of NS5B is defective, *trans*-complementation can succeed if functional NS5B is supplied to the defective system as a member of a separate NS3-NS5B polyprotein construct (10, 15). Based on this observation we constructed models to represent two novel mechanisms for the interaction between viral RNA and NS5B which would allow for

Accepted Manuscript Posted Online

Journal of Virology

JVI

differing *cis*- or *trans*-activities of NS5B, as alternatives to the mechanism proposed by Binder et al (Figure 2A) (8).

In Alternative Mechanism 1, we hypothesize that the plus-strand RNA molecule remains bound to NS5B throughout the entire cleavage process (Figure 2B). At the end of the cleavage steps, NS5A is released—as it can be supplied in *trans*—and a complex of RNA with NS5B remains. This RNA/NS5B complex then associates with the host factor/NS5A complex (see above NS5A section), and these two are imported into the VMS in a second order reaction. This mechanism suggests that NS5B *trans*-complement would only occur if the wild-type NS5B protein was able to replace the defective NS5B that is translated from the RNA. This is one of the possibilities posed by Kazakov et al. in their *trans*-complementation study (15).

The other possibility proposed by the Kazakov et al. study is that the plus-strand RNA is transferred from the ribosome that produced a defective polyprotein to a functional set of the NS3-NS5B proteins for replication (15). For our model, the implication of this mechanism is that the plus-strand RNA only associates with a particular NS5B immediately prior to trafficking into the VMS. Therefore, in Alternative Mechanism 2, we hypothesize that the plus-strand RNA molecule is not bound to NS5B through the processing step and can instead continue to translate more polyprotein (Figure 1B). In this model, the RNA is required to associate with a free NS5B molecule to form the RNA/NS5B complex, which is then imported into the VMS as in Alternative Mechanism 1. Of note, Alternative Mechanism 2 allows for a larger accumulation of excess viral proteins early in the infection, which is consistent with previous research which has shown that most viral proteins do not enter the VMS (38, 39). Both these models were fit to the experimental data to determine which was able to produce a better fit.

Downloaded from http://jvi.asm.org/ on March 26, 2018 by LANL Research Library

Journal of Virology

Accepted Manuscript Posted Online

Journal of Virology

JVI

Journal of Virology

Downloaded from http://jvi.asm.org/ on March 26, 2018 by LANL Research Library

VMS structure and replication mechanism. Early HCV imaging studies established that the structure of the VMS consists of a membranous web that forms a protective double membrane system around the viral replication complexes (19, 40). Consistent with this, our initial fitting efforts showed a tendency for the VMS degradation rate in our model to drop to zero to achieve a better fit. As this is consistent with prior studies that have shown complete nuclease/protease resistance within the replicative compartment (38, 39), we set the VMS degradation rate to 0.001—a low but non-zero value in the interest of biological accuracy—for our simulation.

Notably, recent imaging and 3D modeling of HCV-induced membrane alterations has indicated that the VMS contains multiple, smaller individual replication complexes enclosed in distinct vesicle (41) consistent with previous stoichiometry indicating that individual HCV replication complexes contain a single minus-strand RNA and ten positive-strand RNAs (45). The implication of this hypothesis for an HCV model is that, rather than treating the VMS as a single large pool of viral protein and template RNA for replication, each reaction inside the VMS would be first order and would not depend on the larger VMS concentration of proteins or RNAs. For our model, only one reaction must change to achieve this: the formation of the dsRNA/NS5B complex to produce new plus-strand RNA, which is originally designed as a second order reaction. The broader implication of this first-order model is that there will be a smaller difference between early-lifecycle and late-lifecycle association of the R_{ids} complex, as the total amount of NS5B will have no bearing on this reaction rate.

Experimental Monitoring of HCV Lifecycle Kinetics

To train the mathematical model on the early infection dynamics of HCV, we performed experiments to quantify intracellular and extracellular viral parameters from infection initiation to steady state. For these experiments, Huh7 cells were inoculated with JFH-1 HCVcc at an MOI

Accepted Manuscript Posted Online

Journal of Virology

JVI

Journal of Virology

Downloaded from http://jvi.asm.org/ on March 26, 2018 by LANL Research Library

of 3 for 3 hours. Parallel samples were collected at various time points to count cell number and measure levels of extracellular HCV titer, and intracellular HCV and GAPDH RNA, as well as the viral and cellular proteins core, NS3, and actin. Immunofluorescent staining at 24 hours post-inoculation before progeny virus production is observed indicated that this inoculation resulted in 95% of cells in the culture being infected (See Methods).

HCV RNA and cellular GAPDH mRNA were measured by RTqPCR and used to calculate HCV RNA copies per cell. As typically observed after a high MOI viral infection, the RNA accumulation kinetics showed a slight decline of HCV RNA from 3 to 6 hours post-inoculation, indicative of the degradation of excess non-infectious input viral RNA, before evidence of RNA amplification was detected at 9 hours. This was followed by exponential increase in viral RNA thereafter (Figure 3A). The presence of infectious virus was monitored by titration of the culture media (Figure 3B). The infectious virus detected at the 3 hour time point is the virus remaining from the inoculum that had not initiated infection prior to its removal. After removal of the inoculum at 3 hours, residual infectious virus declined slowly. The first increase in extracellular infectious virus was detected at 24 hours, presumably indicating the accumulation of secreted progeny virus, which subsequently increased exponentially until the end of the experiment.

In parallel wells, we measured intracellular core, NS3, and β-actin protein by Western blot (Figure 3C). Core was detected at 3 hours post-inoculation, but levels slowly declined until 15 hours post-inoculation, consistent with the detection of input core and subsequent degradation before any new accumulation of core could be detected (Figure 3A). In contrast, NS3 was barely detectable at 3 hours post-inoculation but immediately started to accumulate until ~12 hours post-inoculation when HCV RNA amplification becomes exponential. NS3 levels plateaued from 12 to 24 hours post-inoculation before beginning to increase again coincident with the first

Accepted Manuscript Posted Online

Journal of Virology

JVI

Journal of Virology

Downloaded from http://jvi.asm.org/ on March 26, 2018 by LANL Research Library

269 detectable accumulation of core and the first detectable progeny virus secretion (Figure 3B). The
270 levels of β-actin were used to normalize protein levels across all time points.

271 **HCV protein degradation kinetics.** Because core and NS3 did not accumulate with the same
272 kinetics during the viral lifecycle (Figure 3A), we proceeded to determine the degradation rate of
273 these proteins at two time points in the viral lifecycle. For this experiment, Huh7 cells were
274 infected with HCVcc at an MOI of 3. Cycloheximide, a protein translational inhibitor, was
275 introduced at either 12 hours post-inoculation (at the beginning of HCV RNA replication, but
276 prior to progeny virion production) or 27 hours post-inoculation (coincident with active progeny
277 virion assembly) to examine differences between degradation rates at these time points. After the
278 addition of cycloheximide, protein lysates were harvested from parallel cultures at one-hour
279 intervals and levels of core and NS3 were measured by Western blot to monitor the decay of the
280 pre-existing pool of each of these proteins. In the absence of new protein synthesis, NS3 levels
281 remained relatively stable for 3 hours at both time intervals (Figure 4A) with similar degradation
282 rates of 0.11 h^{-1} (12-15 hours post-inoculation) and 0.05 h^{-1} (27-30 hours post-inoculation)
283 (Figure 4B). In contrast, while core protein remained detectable during the later cycloheximide
284 treatment it rapidly disappeared during the 12-15 hours post-inoculation time interval (Figure
285 4A) corresponding to a rapid degradation rate of 0.61 h^{-1} early in infection and a significantly
286 slower 0.10 h^{-1} degradation rate later in infection (Figure 4B). While core protein is known to
287 exist in different functional populations within the cells (e.g. unassembled versus assembled),
288 our measurement of total core degradation rate represents an average of all the core present in the
289 cells and presumably the changes average degradation observed reflect the relative difference in
290 the size of these different core populations early versus later in the viral lifecycle. The NS3 data
291 was incorporate by fitting the degradation rate for the nonstructural proteins (k_{degNS}) in the model

Accepted Manuscript Posted Online

Journal of Virology

JVI

using these calculated rates as upper and lower bounds. To address the core protein degradation rate, we evaluated models with varying core degradation rates (as described below), that were consistent with the new degradation data available. The core degradation rate (k_{degs}) was set at 0.61 h^{-1} from 0 to 21 hours, the first time point where we observe significant viral production, and at 0.10 h^{-1} from 21 hours onward.

Comparison of Model Mechanism

To test the alternative proposed HCV lifecycle mechanisms incorporated into our model, our empirically measured intracellular HCV RNA, virion production, and NS3 and core protein levels were fit to the model species total viral RNA, virions produced, NS3/4A, and structural protein, respectively. Total viral RNA is defined as the sum of all intracellular HCV RNA molecules contained within the model species R_p^{cyt}, R_p^{VMS}, dsRNA (2 molecules), TC, Rp5B, R_{ip}, and R_{ids} (2 molecules) (Table 2).

Non-Structural Protein *cis*/*trans* Behavior. Our two hypothesized model variants for *cis*-/*trans*-acting non-structural proteins, described previously as Alternative Mechanism 1 and Alternative Mechanism 2 as well as the model based on the *cis*-acting protein mechanism proposed by Binder et al. and used by Clausznitzer et al. (8, 12) were fit to our experimental kinetic data to assess the separate mechanisms for *cis*- and *trans*-acting NS protein functions. Models fits were evaluated using the Akaike Information Criterion (AIC), which evaluates goodness of fit against model complexity, with lower scores indicating a better fit.

For the Binder/Clausznitzer mechanism, the fitted model had an AIC of 530 (Figure 5A). Alternative Mechanism 1 yielded an AIC of 983 (Figure 5B) and Alternative Mechanism 2

Downloaded from http://jvi.asm.org/ on March 26, 2018 by LANL Research Library

Journal of Virology

Accepted Manuscript Posted Online

Journal of Virology

JVI

Journal of Virology

Downloaded from http://jvi.asm.org/ on March 26, 2018 by LANL Research Library

yielded an AIC of 478 (Figure 5C). The Alternative Mechanism 2 AIC is substantially lower than either of the other two indicating a much better model, which is apparent in the qualitative comparison of the plots. For this reason, this dual *cis/trans*-acting protein mechanism was chosen as the best representation for the kinetics of JFH-1 HCVcc infection in Huh7 cells.

Independent Replication Complexes in VMS. To explore the possibility that all replication complex vesicles within the VMS act independently, the reactions within the VMS were modified to be first order with respect to the number of minus-strand RNAs present. As noted previously, this requires only modifying the reaction for the formation of the dsRNA/NS5B complex, so that it no longer depends on the NS5B concentration. This mechanism was evaluated in the final model against the original pooled VMS model structure. The new model fitting produced an AIC of 479 (Figure 6) which is similar to the pooled VMS model (AIC 478), indicating only small differences in qualitative fits. As the fitting parameters for these models are very similar, this structure may warrant further exploration with additional data, despite the fact that we maintained a pooled VMS in the final model.

Variable Core Degradation Rate. To evaluate whether allowing for a variable core degradation rate in the model (as described above) improves the quality of the fit to the experimental data. The final model was refit using a constant degradation rate. Refitting yields a constant degradation rate of 0.28 h^{-1}, and an AIC of 486 indicating a slightly worse model than the variable rate model (Figure 7).

Model Validation

Accepted Manuscript Posted Online

Journal of Virology

JVI

Journal of Virology

Downloaded from http://jvi.asm.org/ on March 26, 2018 by LANL Research Library

To determine whether the model we have constructed is able to predict the infection dynamics of additional experiments, we performed a second set of HCV infection experiments under slightly modified experimental conditions and applied the model. These new experiments were conducted with Huh7 cells infected with a different stock of JFH-1 HCVcc at a higher MOI of 7. Again, intracellular HCV and GAPDH RNA were measured by RT-qPCR, and HCV RNA copies per cell were calculated based on cell number.

To account for inherent biological variability between experiments, model parameters for reactions in which virus-derived species interact with each other, and for which we do not have literature values, were allowed to vary up or down by 10% of their values from fitting the training data. These parameters are k_{Rp5B}, k_{Rip}, and $k_{assembly}$.

Quality of fit was assessed using root mean-squared log error (RMSLE) to allow for comparison across orders of magnitude variation in the data, and for different numbers of data points for the 36-hour versus 48-hour experiments. The validation RNA data achieved an RMSLE of 0.14, which is an improvement on the quality of fit achieved in the original RNA data fitting, which produced an RMSLE of 0.24 (Figure 8). This new fit validates the applicability of our model to experiments independent from our original data set.

Sensitivity Analysis

A parameter sensitivity analysis was conducted using the complex-step derivative approximation for HCV intracellular RNA as well as core and NS3 proteins relative to all model parameters. This method uses differential sensitivity values of the form $\mathrm{d(Model\ Species)/d(parameter)}$ at many time points throughout the simulation interval and integrates these with respect to time to find relative average sensitivity values across the entire simulation (See Methods). These values

Accepted Manuscript Posted Online

Journal of Virology

JVI

Journal of Virology

Downloaded from http://jvi.asm.org/ on March 26, 2018 by LANL Research Library

can be evaluated on a relative basis, e.g. a sensitivity value of 20 corresponds to twice the influence on a fractional change in RNA or protein levels as a sensitivity of 10, when this effect is averaged across the whole simulation period.

For each species, the highest sensitivity is seen primarily for the polyprotein translation rate ($k_{translation}$) and RNA synthesis ($k_{initiation}$ and $k_{replication}$), which is expected as each process directly produces more intracellular viral species (Figure 9). Additionally, we observe elevated sensitivities to the parameters for translation complex formation (k_{TC}), RNA transport to the cytoplasm (k_{outRp}) and, for virion production, particle assembly/egress ($k_{assembly}$). Of the degradation rates the structural protein rate has the largest negative sensitivity for its own levels as well as virion production. For the VMS degradation rate (k_{degVMS}) there is low sensitivity for each species at the low rate we have chosen for our model. The number of virions produced consistently has higher sensitivities than the other model species, indicating that it is the most variable with fluctuations in the viral lifecycle kinetics. The degradation rates produce a consistent negative sensitivity, as expected, given that degradation of viral species will slow the viral lifecycle.

Accepted Manuscript Posted Online

Journal of Virology

JVI

Journal of Virology

Downloaded from http://jvi.asm.org/ on March 26, 2018 by LANL Research Library

Discussion

Evaluating viral protein *cis*-/*trans*-activities creates a more accurate infection model. While experimentally testing whether proteins function in *cis* or *trans* can be complex, modeling different mechanisms against empirical data provides an alternative strategy for investigating such questions. Our comparison of three possible mechanisms for the *cis*-/*trans*-acting behavior of HCV non-structural proteins (Figure 5) demonstrates that the mechanism that offers the greatest *trans*-activity potential—referred to as Alternative Mechanism 2—is the best model for the HCVcc experimental data. In earlier models, the nature of non-structural viral proteins was represented as a *cis*-function in which active translation complex was imported into the VMS alongside a host factor and generalized non-structural protein. However, based on more recent observations suggesting that the non-structural proteins can be complemented as a group *in trans* (15), we have proposed an alternate mechanism in which the cytoplasmic viral RNA does not necessarily remain associated with the proteins that have been translated from it, but can associate with any NS5B protein post-cleavage from the viral polyprotein. Fitting this model to experimental data for total viral RNA, virion production and viral proteins (NS3 and core) demonstrated that this was the best model as quantified by AIC value, suggesting that the assembly of viral replication complexes may exhibit more *trans*-interaction between the viral RNA and proteins than previously thought.

Introducing core protein regulation creates a more physiologically relevant infection model. While HCV proteins are by default translated at the same rate as part of the virally encoded polyprotein, our HCVcc infection protein kinetic data revealed that the accumulation of *de novo* core protein was significantly delayed compared to NS3. Analysis of core and NS3

Accepted Manuscript Posted Online

Journal of Virology

JVI

degradation rates at different times revealed a sharp decrease in core degradation rate between 12 and 27 hours post-inoculation, corresponding to the start of progeny viral production. Notably, incorporating this change in core degradation into our model allowed for a better model than if the core degradation was fit at a constant rate (AIC of 478 versus 486, respectively). This suggests that this change in core stability may be significant to the overall dynamics of the HCV life cycle which may warrant further theoretical and/or experimental exploration. In accordance with this possibility, the virion production of the model shows a substantial negative sensitivity to the core degradation rate (Figure 7).

Further experiment is required to clarify the functional structure of the membranous web. Similar to all known positive strand RNA viruses (43), HCV induces cellular membrane alterations to create a protected space for replication of its genome with accumulating evidence suggesting that this larger membranous structure consists of smaller individual replication complexes enclosed in distinct vesicle (41). Thus, we used our model to compare the previously proposed pooled VMS structure to one in which all vesicles would act independently to determine if either mechanism would more accurately represent the experimental data (Figure 6). This alternate VMS structure produced a model quality virtually equivalent to that of the original mechanism. We cannot conclude which VMS structure may be more biologically relevant as the first-order reaction for independently-acting vesicles does not appear to be a crucial aspect of model. Based on the marginally better model as determined by AIC, as well as the fact that previous replicon models used a pooled VMS, we have kept this pooled mechanism in our final model.

The usefulness of the final model in predicting the dynamics of hepatitis C infections is supported by the quality of fit achieved using a separate set of experimental HCV infection data

Downloaded from http://jvi.asm.org/ on March 26, 2018 by LANL Research Library

Journal of Virology

Accepted Manuscript Posted Online

Journal of Virology

JVI

Journal of Virology

Downloaded from http://jvi.asm.org/ on March 26, 2018 by LANL Research Library

(Figure 8). Fitting this experimental data, while allowing only unknown parameter values for viral self-interaction to vary slightly, yielded a high-quality fit which indicates that our model will be applicable to other sets of experimental data outside of our training set.

Fitting infection data shows parameter changes from previous models and demonstrates areas for future experiment. Many of our model parameter values have been repurposed from a prior study by Binder et al. (8), which fit an intracellular HCV model to data from a genotype 2a subgenomic replicon experiment. This system was developed from a JFH-1 isolate, the same virus clone we have used in our experiments. However, upon fitting, some model parameters involved with translation ($k_{translation}$, $k_{cleavage}$, and number of available ribosomes) were found to vary markedly from the analogous parameters in the previous model, despite the translation mechanism remaining largely intact between models. This observation may reflect a limitation in directly applying HCV replicon model parameter estimates to predict HCV infection dynamics, the significant degree of variability/permissiveness between cell lines used, which has been documented in the HCV literature (8, 44), or perhaps the difference between transfection of large quantities of HCV replicon RNA into cells versus the more authentic HCVcc infections we performed where it is believed that HCV replication begins from a single viral RNA. While such variability might in some cases make it difficult to utilize a single model across experimental systems, when comparing sufficiently similar experimental systems (e.g. replicon-to-replicon or infection-to-infection) modeling can potentially help postulate what might make one cell line more permissive (as demonstrated by Binder et al.,) or one viral clone more robust (8).

Sensitivity analysis indicates that viral translation and replication are the critical steps in altering the viral production rate. In terms of the steady-state levels and accumulation kinetics for total intracellular viral RNA, core, NS3, and virion production, the parameters that exhibited

Accepted Manuscript Posted Online

Journal of Virology

JVI

the most influence in this infection model were found to be $k_{translation}$ (polyprotein translation rate), $k_{initiation}$ (minus-strand synthesis), and $k_{replication}$ (plus-strand synthesis). These sensitivities highlight the major synthesis steps of the viral lifecycle, an expected observation as these are the processes that drive production of the RNA and protein species we are following experimentally. The high sensitivity of model species to the plus and minus-strand synthesis steps is also consistent with findings presented by Binder et al. in their analysis of the replicon mathematical model, which concluded that the replication vesicles were the most influential component of the system (8). Additional information gained from the expansion of the model to describe the full HCV life cycle indicates that virion production exhibits a high magnitude of sensitivity to several model parameters. Along with translation and replication we observe a high sensitivity to particle assembly/egress ($k_{assembly}$) and a low negative sensitivity to degradation of core protein (k_{degS}). The two parameters would be expected to influence virion production and raise the possibility of therapeutic targets within the viral lifecycle to decrease HCV output.

Conclusions. In this study, we have presented a model of the hepatitis C virus infection lifecycle that both accurately represents the dynamics of the viral infection system and may be used to probe the functions and behaviors of individual viral proteins produced by the HCV genome. This model improves on the fitting quality of previous mechanisms, confirms distinct regulation of the levels of the HCV structural versus nonstructural viral proteins during the viral lifecycle, and helps to elucidate the functional interaction of different viral proteins with the host cell. While our final model (Figure 1) describes the infection data better than previous models, there is still room for improvement in the fits. Importantly, the nature of the fit discrepancies observed between the model simulation and the experimental data raises some mechanistic ideas that could be explored in future work. As such, this model can now be used to guide future

Downloaded from http://jvi.asm.org/ on March 26, 2018 by LANL Research Library

Journal of Virology

experimentation and will allow us to continue to improve our understanding of HCV infection dynamics. Future experimental efforts could also help to clarify the precise kinetics and mechanisms that are approximated by the differential equations posed in this mathematical model. Moreover, the experimental testing of model predictions for viral production and lifecycle sensitivities may aid in efforts to understand the lifecycle and to target antiviral drugs and treat chronic hepatitis C infection.

Accepted Manuscript Posted Online
Journal of Virology
JVI
Journal of Virology
Downloaded from http://jvi.asm.org/ on March 26, 2018 by LANL Research Library

Accepted Manuscript Posted Online

Journal of Virology

JVI

Downloaded from http://jvi.asm.org/ on March 26, 2018 by LANL Research Library

Materials and Methods

Experimental Measurements of HCV Replication

Cells. Huh7 cells were obtained from Dr. Francis Chisari (The Scripps Research Institute, La Jolla, CA) (45) and passaged in complete Dulbecco's modified Eagle's medium (cDMEM) supplemented with 10% fetal bovine serum (FBS) (Hyclone), 100 units/ml penicillin, 100 mg/ml streptomycin, 2 mM L-glutamine (Invitrogen). Cells were incubated at 37°C under 5% CO_2.

Virus. The plasmid containing the full-length HCV JFH-1 genome (pUC-JFH1) was provided by Dr. Takaji Wakita (National Institute of Infectious Diseases, Tokyo, Japan) (46). The stocks of HCVcc used for experiments were generated as described previously (47).

HCVcc infections. For HCV infection time course experiments, Huh7 cells were plated and grown overnight to a cell count of 8,000 for the training set experiments and 10,000 for the validation experiments. The next day cultures were inoculated with HCVcc at an MOI of 3 (training) or an MOI of 7 (validation), defining this moment as t = 0 hours. At 3 hours post-inoculation, the viral inoculum was removed, cells were rinsed, and fresh media was added. We then harvested media and cell lysates from triplicate wells for titer analysis and RNA, respectively and cell lysate from an additional triplicate wells for protein analysis at the indicated time points. To monitor the percentage of cells infected, immunofluorescent staining for HCV NS5A was performed at 24 hours post-inoculation before any significant progeny virus release was detected.

RNA isolation and RTqPCR analysis. For RNA extraction, cell lysates were harvested in 200 µL Nucleic Acid Purification Lysis solution (Applied Biosystems) from 3 replicate wells. Total cellular RNA was purified using an ABI PRISM™ 6100 Nucleic Acid PrepStation (Applied

Journal of Virology

Accepted Manuscript Posted Online

Journal of Virology

JVI

Journal of Virology

Downloaded from http://jvi.asm.org/ on March 26, 2018 by LANL Research Library

492 Biosystems), as per the manufacturer's instructions. Extracellular RNA was isolated by adding a
493 5/3x guanidine thiocyanate (GTC) solution to the culture media to obtain a 1xGTC lysate, which
494 was subsequently processed using standard protocols (48). One microgram of RNA was used for
495 cDNA synthesis using random primer reverse transcription (Applied Biosystems), followed by
496 RTqPCR using FastStart Universal SYBR Green master mix (Roche Applied Sciences,
497 Indianapolis, IN). The following qPCR primers were used: HCV primers 5'-GCC TAG CCA
498 TGG CGT TAG TA -3' (sense) and 5'- CTC CCG GGG CACTCG CAA GC-3' (anti-sense) and
499 human GAPDH 5'-GAA GGT GAA GGT CGG AGT C-3' (sense) and 5'-GAA GAT GGT GAT
500 GGG ATT TC-3' (anti-sense). HCV RNA copies were quantified relative to a standard curve
501 comprised of serial dilutions of the pJFH-1 plasmid and normalize to cellular GAPDH RNA.

502 **RNA per-cell quantification.** Cell counts were performed at a subset of time points and relative
503 levels of GAPDH mRNA, a cellular housekeeping gene, was assayed at all points confirming
504 that cell count did not change over the course of the experiment, confirming that in this
505 experimental model system in the time frame assayed there is no cell death observed. This
506 constant cell count, multiplied by the 95% of cells determined to be infected based on an HCV
507 NS5A immunofluorescence assay (Figure 10), was used to determine the approximate number of
508 infected cells throughout the experiment. RT-qPCR data, scaled to a per-well basis and divided
509 by the number of infected cells, was then used to calculate the average copies of HCV RNA per
510 infected cell.

511 **Extracellular infectivity titration assay.** Experimental supernatant samples were serially
512 diluted 10-fold in cDMEM and 100 µl was used to infect naïve 96-well Huh7 cell cultures. The
513 inoculum was incubated with cells for 24 h at 37°C and then overlayed with 150 µl cDMEM
514 containing 0.5% methylcellulose (w/v) (Fluka BioChemika, Switzerland) to give a final

Accepted Manuscript Posted Online

Journal of Virology

JVI

Journal of Virology

Downloaded from http://jvi.asm.org/ on March 26, 2018 by LANL Research Library

515 concentration of 0.3% methylcellulose. Seventy-two h p.i., medium was removed, cells were
516 fixed with 4% paraformaldehyde (Sigma) and immunohistochemical staining for HCV E2-
517 positive foci was performed as previously described (47).

518 **Immunofluorescent HCV NS5A staining.** Cells were fixed with 4% paraformaldehyde (Sigma)
519 for 20 minutes and rinsed with 1xPBS. HCV NS5A was detected by incubation at room
520 temperature with 1X PBS containing 0.5% (v/v) Triton X-100 and 3% (w/v) BSA and a 1:500
521 dilution of the monoclonal NS5A antibody 9E10 (a gift from Dr. Charles Rice, Rockefeller
522 University, New York, NY), followed by a 1 h incubation with a 1:500 dilution of an HRP-
523 conjugated anti-mouse antibody (Vector Labs, CA) and Hoescht dye diluted 1:3000 before
524 subsequent detection with AEC substrate (BD Biosciences). Cells were washed with dH_2O.
525 Staining was photographed using a Nikon TE2000U microscope (Nikon Instruments).

526 **Western blot.** Cells were harvested at various time points from triplicate wells in 1.25% Triton
527 X-100 lysis buffer (Triton X-100, 50mM Tris-HCl, pH7.5, 150mM NaCl, 2mM EDTA)
528 supplemented with a protease inhibitor cocktail (Roche Applied Science, Indianapolis, IN) and
529 pooled. Thirty-five micrograms of pooled protein were resolved by 10% SDS-PAGE and
530 transferred to Hybond nitrocellulose membranes. Membranes were blocked with 5% nonfat milk
531 for 1 hour followed by an overnight incubation with primary antibodies anti-core (clone C7-50,
532 Santa Cruz Biotechnologies, Santa Cruz, CA) or anti-NS3 (clone 9-G2, Watertown, MA) each at
533 a 1:500 dilution. Membranes were washed 3 times with 1X TBS containing 0.05% Tween20
534 (v/v), and then incubated with secondary HRP-conjugated goat anti-mouse (Pierce, Rockford,
535 IL) at 1:4000 dilution for 30 minutes. As a loading control, membranes were incubated with a
536 HRP-conjugated β-actin monoclonal antibody at a 1:25000 dilution. SuperSignal West Pico
537 Chemiluminescent substrate was used to detect bound antibody complexes (Pierce, Rockford,

Accepted Manuscript Posted Online

Journal of Virology

JVI

Journal of Virology

Downloaded from http://jvi.asm.org/ on March 26, 2018 by LANL Research Library

538 IL) and the resulting signal was quantified by densitometry using OptiQuant™ Image Analysis
539 software (Perkin Elmer, Waltham, MA).

540 **Protein per-cell quantification.** Absolute quantities of core protein per cell were estimated
541 based on the initial virus input. Specifically, because replication is not detectable until 9 hours
542 post-inoculation and translation is minimum at 3 hours post-inoculation, we assumed that the
543 HCV RNA and vast majority core protein present at 3 hours post-inoculation represented input
544 virions. Therefore, using an estimated HCV particle core:RNA ratio from the literature of 180:1
545 (49), we estimated the number of core molecules based on our quantitative measurement of HCV
546 RNA. The number of core molecules and NS3 molecules at all time points were then scaled to
547 the 3-hour time point based on the relative Western blot signal obtained, under the assumption
548 that the measured DLU quantities for the two proteins correspond to a roughly 1:1 molar ratio.

549 **Protein degradation experiments.** Huh7 cells were infected with HCVcc at an MOI of 3, and
550 cycloheximide was introduced at a concentration of 50 μg/mL to stop protein synthesis at either
551 12 or 27 hours post-inoculation. After the addition of cycloheximide, protein was harvested from
552 parallel cultures at 1 hour increments for 3 hours to monitor protein levels by Western blot.
553 Western blots were quantified and core protein and NS3 levels were normalized to cellular actin
554 levels. Degradation rates were calculated by fitting a trend line to the decaying quantities of
555 protein after translation had been halted.

556 **Mathematical Model Equations.** The mathematical model that describes the infection system
557 of HCV consists of 17 equations one for each individual species within the system. The system is
558 divided into the general cytoplasmic compartment versus a specific cytoplasmic VMS
559 compartment, which are distinct in their functions as well as degradation rates, with VMS-
560 enclosed species being resistant to protease/nuclease degradation. The cytoplasm contains 11

Accepted Manuscript Posted Online

Journal of Virology

JVI

species of the model while the VMS contains 5. The defining equations are shown in Table 2. In most cases species are referred to by the abbreviation presented in the model schematic (Figure 1B). The exceptions are R_p (plus-strand RNA), HFC (host factor/NS5A complex), Rp5B (RNA/NS5B complex), R_{ip} (minus-strand synthesis complex), R_{ids} (plus strand synthesis complex), and V_{out} (extracellular virions). All model parameters are displayed in Table 1.

Model Parameter Estimation.

Model parameters were obtained through a combination of fitting and estimations based on the literature and previous models. The Dahari study (7) averaged steady state values from several HCV genotype 1b subgenomic replicon to fit its model, while the Binder model (8) used genotype 2a (JFH-1, as in our study) subgenomic replicon constructs for its experiments.

Translation phase parameters. Translation phase parameters encompass those involved in translation and polyprotein processing (Table 1). The parameter k_{TC} was estimated in previous models (7, 8) simulating subgenomic replicon experiments, and this estimate was used in our model. For $k_{translation}$, the prior models' value of 100 polyproteins per hour was used as an initial estimate but was found to be insufficient. An upper bound of 180 polyproteins per hour was calculated based on an estimate of 10 amino acids per second, within the range observed for eukaryotic cells (50, 51), and the assumption of polyribosomes distributing across the 9,000-nt viral RNA ORF at the same proportion as estimated by Dahari et al. in their replicon model (7). The cleavage parameter $k_{cleavage}$ was calculated based on fitting.

Replication phase parameters. Replication phase parameters encompass those involved in VMS import, replication complex formation, and RNA synthesis (Table 1). The rates for viral RNA synthesis were calculated previously from the literature (6, 52, 53) in earlier HCV models,

Downloaded from http://jvi.asm.org/ on March 26, 2018 by LANL Research Library

Journal of Virology

Accepted Manuscript Posted Online

Journal of Virology

JVI

Journal of Virology

Downloaded from http://jvi.asm.org/ on March 26, 2018 by LANL Research Library

583 and was held constant on a per-nucleotide basis for building this model, as it is a trait inherent to
584 the NS5B polymerase. For the parameter k_{Rids}, which exists with perfect analogy in previous
585 models, the prior value was used. The parameter estimate for k_{Rids} was found to be adequate for
586 the infection model after fitting. The value for k_{Rip}, which changes from a third-order reaction in
587 previous models to a second order reaction in ours, was calculated with fitting. The new
588 parameters k_{HFC} and k_{Rp5B} were also calculated using model fitting to the training data.

589 **Transport parameters.** These parameters involve cellular import/export and VMS export of
590 RNA. The VMS export parameter (k_{outRp}) was present in previous models, and this value was
591 used. The viral particle assembly rate constant ($k_{assembly}$) was initially estimated using the similar
592 second order virion production parameter used in the previous multi-scale model (12). From
593 fitting this parameter guess, however, this was found to be too high of a value, likely due to the
594 fact that our model incorporates 180 structural protein molecules into each secreted particle,
595 while the previous model used only one. We estimated $k_{assembly}$ through data fitting.

596 **Host species**. Ribosomes, host factor, and extracellular RNA were defined as host species. The
597 number of available ribosomes and host factors were initially taken to be equal to the quantities
598 used in previous models, but it was soon observed in fitting that a higher quantity of available
599 ribosomes was more appropriate by fitting the experimental data.

600 **Degradation rates.** The degradation rate for nonstructural proteins was estimated using the
601 values calculated for the degradation rate of NS3 at the 12- and 27-hour time points in the viral
602 lifecycle (Figure 3). These degradation rates, 0.11 h^{-1} and 0.05 h^{-1}, were used as the upper and
603 lower bounds for fitting the protein degradation rates, and the fitting algorithm chose 0.11 h^{-1} as
604 the overall nonstructural protein degradation rate. This estimation of degradation rates was found
605 to be acceptable for our model after fitting, and aided in the reduction of degrees of freedom in

Accepted Manuscript Posted Online

Journal of Virology

JVI

Journal of Virology

Downloaded from http://jvi.asm.org/ on March 26, 2018 by LANL Research Library

the fitting process. Degradation rates for all species in the VMS were estimated to be zero based on previous studies showing complete protease/nuclease resistance for species in the replicative compartment (38, 39). Cytoplasmic RNA degradation rate (k_{degRp}) was fit to our data after using the value from the Binder model as an initial estimate. As described above, two separate core degradation rates were calculated for the first and second phases of the lifecycle (prior to and after virion production starting at 21 hours).

Simulation Procedure. Simulation and data fitting were carried out using MATLAB 2016b with the SimBiology package to construct a model of ordinary differential equations according to those presented above (https://www.colorado.edu/UCB/chatterjeelab/HCVmodel.html). The "Fit Data" task was used to estimate model parameters using the stiff *ode15s* solver with absolute and relative tolerances set to 10^{-7}. This fitting was performed in an iterative fashion, as the model contains too many parameters to be efficiently estimated simultaneously. The model was fit to experimental data for RNA, core, and NS3 simultaneously with a proportional error model described by Equation 18. This was chosen based on the large order-of-magnitude variation in the data across the experiments.

$$y_{exp} = y_{sim} + b * abs(y_{sim}) * error \tag{18}$$

A tolerance of 1E-8 was chosen for termination of the data fitting procedure for the step-change in estimated parameters and the function value, and 1E-6 for the first order optimality.

Sensitivity Analysis. The "Sensitivity Analysis" task of the SimBiology package was used to estimate parameter sensitivities for RNA, NS3, core protein and virion production. This task uses the complex-step derivative approximation, which is often used for metabolic systems (54–56). Full de-dimensionalization of the analysis was used to be able to compare parameters of widely-

Accepted Manuscript Posted Online

Journal of Virology

JVI

Journal of Virology

Downloaded from http://jvi.asm.org/ on March 26, 2018 by LANL Research Library

varying orders-of-magnitude. This calculation for complex-step derivative sensitivities can be represented by the following equations for each parameter:

$$f' = \frac{df}{d(k_{reaction})} \tag{19}$$

$$f(k_{reaction}, t) = species\ X\ per\ cell \tag{20}$$

$$Sensitivity = \int_0^{t_{final}} f'(t)\, dt \tag{21}$$

Identifiability Analysis. We used the program GenSSI (57) to test our model for global structural identifiability on the parameters that were subjected to our model fitting to examine the uniqueness of our solution. These parameters are k_{TC}, $k_{translation}$, $k_{cleavage}$, k_{HFC}, k_{Rp5B}, k_{Rip}, $k_{assembly}$, and k_{degRp}. Parameters for which experimental or literature values were used were fixed in this analysis and were not considered for identifiability. Identifiability analysis by GenSSI, using iterative Lie derivatives to calculate successive identifiability tableaus as described previously by Chis et al. and Balsa-Canto et al. (Figure 11) (57, 58), determines that the parameters k_{TC}, $k_{translation}$, $k_{cleavage}$, k_{Rp5B}, and k_{degRp} are globally identifiable and that $k_{HFC,}$ k_{Rp5B}, and k_{Rip} are non-identifiable. The former indicates that a unique solution exists for the parameters while the latter indicates that we cannot be sure of a unique solution for these parameters. For this reason, we avoid drawing conclusions based on those parameter values. As our model's goal is primarily to evaluate model structure and add biological accuracy to the protein mechanisms we have concluded that this degree of identifiability is enough to provide a useful model. To calculate values of model parameters with confidence more experimental data would be necessary.

Accepted Manuscript Posted Online

Journal of Virology

JVI

Journal of Virology

Downloaded from http://jvi.asm.org/ on March 26, 2018 by LANL Research Library

Acknowledgments

Portions of this work were performed under the auspices of the U.S. Department of Energy under contract DE-AC52-06NA25396. This work was funded by National Institutes of Health grants R01-AI078881 (SLU), R01-OD011095, R01-AI028433, R01-AI116868 (ASP), and University of Colorado Start-up grant and DARPA Young Faculty Award (D17AP00024) to AC.

Accepted Manuscript Posted Online

Journal of Virology

JVI

Journal of Virology

Downloaded from http://jvi.asm.org/ on March 26, 2018 by LANL Research Library

References

1. 2017. Global Hepatitis Report. World Health Organization.
2. Burstow NJ, Mohamed Z, Gomaa AI, Sonderup MW, Cook NA, Waked I, Spearman CW, Taylor-Robinson SD. 2017. Hepatitis C treatment: Where are we now? Int J Gen Med 10:39–52.
3. Chatterjee A, Guedj J, Perelson AS. 2012. Mathematical modelling of HCV infection: What can it teach us in the era of direct-acting antiviral agents? Antivir Ther 17:1171–1182.
4. Chatterjee A, Smith PF, Perelson AS. 2013. Hepatitis C Viral Kinetics. The Past, Present, and Future. Clin Liver Dis 17:13–26.
5. 2016. Hepatitis C FAQs for the Public. CDC.
6. Lohmann V, Körner F, Koch J, Herian U, Theilmann L, Bartenschlager R. 1999. Replication of subgenomic hepatitis C virus RNAs in a hepatoma cell line. Science 285:110–113.
7. Dahari H, Ribeiro RM, Rice CM, Perelson AS. 2007. Mathematical modeling of subgenomic hepatitis C virus replication in Huh-7 cells. J Virol 81:750–60.
8. Binder M, Sulaimanov N, Clausznitzer D, Schulze M, H??ber CM, Lenz SM, Schl??der JP, Trippler M, Bartenschlager R, Lohmann V, Kaderali L. 2013. Replication Vesicles are Load- and Choke-Points in the Hepatitis C Virus Lifecycle. PLoS Pathog 9.
9. Novak JE, Kirkegaard K. 1994. Coupling between genomic translation and replication in an RNA virus. Genes and Devel 8:1726–1737.
10. Appel N, Herian U, Bartenschlager R, Appel N, Herian U, Bartenschlager R. 2005. Efficient Rescue of Hepatitis C Virus RNA Replication by trans -Complementation with Nonstructural Protein 5A Efficient Rescue of Hepatitis C Virus RNA Replication by trans -Complementation with Nonstructural Protein 5A. J Virol 79:896–909.
11. Khromykh AA, Sedlak PL, Westaway EG. 2000. cis- and trans-Acting Elements in Flavivirus RNA Replication. J Virol 74:3253–3263.
12. Clausznitzer D, Harnisch J, Kaderali L. 2015. Multi-scale model for hepatitis C viral load kinetics under treatment with direct acting antivirals. Virus Res 218:96–101.
13. Bartenschlager R, Ahlborn-Laake L, Mous J, Jacobsen H. 1994. Kinetic and structural analyses of hepatitis C virus polyprotein processing. J Virol 68:5045–5055.
14. Lin C, Pragai BM, Grakoui A, Xu J, Rice CM. 1994. Hepatitis C virus NS3 serine proteinase: trans-cleavage requirements and processing kinetics. J Virol 68:8147–8157.
15. Kazakov T, Yang F, Ramanathan HN, Kohlway A, Diamond MS, Lindenbach BD. 2015. Hepatitis C Virus RNA Replication Depends on Specific Cis- and Trans-Acting Activities of Viral Nonstructural Proteins. PLoS Pathog 11:1–30.

Accepted Manuscript Posted Online

Journal of Virology

JVI

Journal of Virology

Downloaded from http://jvi.asm.org/ on March 26, 2018 by LANL Research Library

690 16. Moradpour D, Penin F. 2013. Hepatitis C Virus Proteins: From Structure to Function, p.
691 113–142. *In* Bartenschlager, R (ed.), Hepatitis C Virus: From Molecular Virology to
692 Antiviral Therapy. Springer-Verlag, Berlin.

693 17. Morikawa K, Lange CM, Gouttenoire J, Meylan E, Brass V, Penin F, Moradpour D. 2011.
694 Nonstructural protein 3-4A: The Swiss army knife of hepatitis C virus. J Viral Hepat
695 18:305–315.

696 18. Pietschmann T, Lohmann V, Rutter G, Kurpanek K, Bartenschlager R. 2001.
697 Characterization of Cell Lines Carrying Self-Replicating Hepatitis C Virus RNAs. J Virol
698 75:1252–1264.

699 19. Egger D, Wölk B, Gosert R, Bianchi L, Blum HE, Moradpour D, Bienz K. 2002.
700 Expression of hepatitis C virus proteins induces distinct membrane alterations including a
701 candidate viral replication complex. J Virol 76:5974–84.

702 20. Gouttenoire J, Penin F, Moradpour D. 2010. Hepatitis C virus nonstructural protein 4B: a
703 journey into unexplored territory. Rev Med Virol 20:117–129.

704 21. Paul D, Romero-Brey I, Gouttenoire J, Stoitsova S, Krijnse-Locker J, Moradpour D,
705 Bartenschlager R. 2011. NS4B self-interaction through conserved C-terminal elements is
706 required for the establishment of functional hepatitis C virus replication complexes. J
707 Virol 85:6963–6976.

708 22. Bartenschlager R, Lohmann V, Penin F. 2013. The molecular and structural basis of
709 advanced antiviral therapy for hepatitis C virus infection. Nat Rev Microbiol 11:482–496.

710 23. Tellinghuisen TL, Marcotrigiano J, Rice CM. 2005. Function follows form: The structure
711 of the N-terminal domain of HCV NS5A. Hepatology 42:732–735.

712 24. Appel N, Zayas M, Miller S, Krijnse-Locker J, Schaller T, Friebe P, Kallis S, Engel U,
713 Bartenschlager R. 2008. Essential role of domain III of nonstructural protein 5A for
714 hepatitis C virus infectious particle assembly. PLoS Pathog 4.

715 25. Tellinghuisen TL, Foss KL, Treadaway JC, Rice CM. 2008. Identification of residues
716 required for RNA replication in domains II and III of the hepatitis C virus NS5A protein. J
717 Virol 82:1073–1083.

718 26. Evans MJ, Rice CM, Goff SP. 2004. Phosphorylation of hepatitis C virus nonstructural
719 protein 5A modulates its protein interactions and viral RNA replication. Proc Natl Acad
720 Sci 101:13038–13043.

721 27. Hanoulle X, Badillo A, Wieruszeski JM, Verdegem D, Landrieu I, Bartenschlager R,
722 Penin F, Lippens G. 2009. Hepatitis C virus NS5A protein is a substrate for the peptidyl-
723 prolyl cis/trans isomerase activity of cyclophilins A and B. J Biol Chem 284:13589–
724 13601.

725 28. Kaneko T, Tanji Y, Satoh S, Hijikata M, Asabe S, Kimura K, Shimotohno K. 1994.
726 Production of Two Phosphoproteins from the NS5A Region of the Hepatitis C Viral
727 Genome. Biochem Biophys Res Commun 205:320–326.

728 29. Reiss S, Rebhan I, Backes P, Romero-Brey I, Erfle H, Matula P, Kaderali L, Poenisch M,

Accepted Manuscript Posted Online

Journal of Virology

JVI

Journal of Virology

Downloaded from http://jvi.asm.org/ on March 26, 2018 by LANL Research Library

729 Blankenburg H, Hiet M-S, Longerich T, Diehl S, Ramirez F, Balla T, Rohr K, Kaul A,
730 Schirmacher P, Lohmann V, Bartenschlager R. 2011. Recruitment and activation of a lipid
731 kinase by NS5A is essential for integrity of the membranous replication compartment.
732 Cell Host Microbe 9:32–45.

733 30. Verdegem D, Badillo A, Wieruszeski JM, Landrieu I, Leroy A, Bartenschlager R, Penin F,
734 Lippens G, Hanoulle X. 2011. Domain 3 of NS5A protein from the hepatitis C virus has
735 intrinsic α-helical propensity and is a substrate of cyclophilin A. J Biol Chem 286:20441–
736 20454.

737 31. Guedj J, Yu J, Levi M, Li B, Kern S, Naoumov N V, Perelson AS. 2014. Modeling viral
738 kinetics and treatment outcome during alisporivir interferon-free treatment in hepatitis C
739 virus genotype 2 and 3 patients. Hepatology 1706–1714.

740 32. Liu Z, Yang F, Robotham JM, Tang H. 2009. Critical role of cyclophilin A and its prolyl-
741 peptidyl isomerase activity in the structure and function of the hepatitis C virus replication
742 complex. J Virol 83:6554–65.

743 33. Romero-Brey I, Berger C, Kallis S, Kolovou A, Paul D, Lohmann V, Bartenschlager R.
744 2015. NS5A domain 1 and polyprotein cleavage kinetics are critical for induction of
745 double-membrane vesicles associated with hepatitis c virus replication. MBio 6:1–12.

746 34. Hwang J, Huang L, Cordek DG, Vaughan R, Reynolds SL, Kihara G, Raney KD, Kao
747 CC, Cameron CE. 2010. Hepatitis C virus nonstructural protein 5A: biochemical
748 characterization of a novel structural class of RNA-binding proteins. J Virol 84:12480–91.

749 35. Huang L, Hwang J, Sharma SD, Hargittai MRS, Chen Y, Arnold JJ, Raney KD, Cameron
750 CE. 2005. Hepatitis C virus nonstructural protein 5A (NS5A) is an RNA-binding protein.
751 J Biol Chem 280:36417–36428.

752 36. Guedj J, Dahari H, Rong L, Sansone ND, Nettles RE, Cotler SJ, Layden TJ, Uprichard
753 SL, Perelson AS. 2013. Modeling shows that the NS5A inhibitor daclatasvir has two
754 modes of action and yields a shorter estimate of the hepatitis C virus half-life. Proc Natl
755 Acad Sci U S A 110:3991–6.

756 37. McGivern DR, Masaki T, Williford S, Ingravallo P, Feng Z, Lahser F, Asante-Appiah E,
757 Neddermann P, De Francesco R, Howe AY, Lemon SM. 2014. Kinetic Analyses Reveal
758 Potent and Early Blockade of Hepatitis C Virus Assembly by NS5A Inhibitors.
759 Gastroenterology 147:453–462.

760 38. Quinkert D, Bartenschlager R, Lohmann V. 2005. Quantitative Analysis of the Hepatitis C
761 Virus Replication Complex. J Virol 79:13594–13605.

762 39. Miyanari Y, Hijikata M, Yamaji M, Hosaka M, Takahashi H, Shimotohno K. 2003.
763 Hepatitis C Virus Non-structural Proteins in the Probable Membranous Compartment
764 Function in Viral Genome Replication. J Biol Chem 278:50301–50308.

765 40. Gosert R, Egger D, Lohmann V, Bartenschlager R, Blum HE, Bienz K, Moradpour D.
766 2003. Identification of the hepatitis C virus RNA replication complex in Huh-7 cells
767 harboring subgenomic replicons. J Virol 77:5487–92.

768 41. Romero-Brey I, Merz A, Chiramel A, Lee J-Y, Chlanda P, Haselman U, Santarella-

Accepted Manuscript Posted Online

Mellwig R, Habermann A, Hoppe S, Kallis S, Walther P, Antony C, Krijnse-Locker J, Bartenschlager R. 2012. Three-Dimensional Architecture and Biogenesis of Membrane Structures Associated with Hepatitis C Virus Replication. PLoS Pathog 8:e1003056.

42. Lohmann V. 2013. Hepatitis C Virus Replication, p. 167–198. *In* Bartenschlager, R (ed.), Hepatitis C Virus: From Molecular Virology to Antiviral Therapy. Springer-Verlag, Berlin.

43. Miller S, Krijnse-Locker J. 2008. Modification of intracellular membrane structures for virus replication. Nat Rev Microbiol 6:363–374.

44. Ye F, Xin Z, Han W, Fan J, Yin B, Wu S, Yang W, Yuan J, Qiang B, Sun W, Peng X. 2015. Quantitative proteomics analysis of the hepatitis C virus replicon high-permissive and low-permissive cell lines. PLoS One 10:1–21.

45. Zhong J, Gastaminza P, Cheng G, Kapadia S, Kato T, Burton DR, Wieland SF, Uprichard SL, Wakita T, Chisari F V. 2005. Robust hepatitis C virus infection in vitro. Proc Natl Acad Sci U S A 102:9294–9.

46. Kato T, Furusaka A, Miyamoto M, Date T, Yasui K, Hiramoto J, Nagayama K, Tanaka T, Wakita T. 2001. Sequence analysis of hepatitis C virus isolated from a fulminant hepatitis patient. J Med Virol 64:334–339.

47. Yu X, Uprichard SL. 2010. Cell-based hepatitis c virus infection fluorescence resonance energy transfer (FRET) assay for antiviral compound screening. Curr Protoc Microbiol 17.5:1–27.

48. Chomczynski P, Sacchi N. 1987. Single-Step Method of RNA Isolation by Acid Guanidinium Thiocyanate-Phenol-Chloroform Extraction. Anal Biochem 162:156–159.

49. Schüttler CG, Thomas C, Discher T, Friese G, Lohmeyer J, Schuster R, Schaefer S, Gerlich WH. 2004. Variable Ratio of Hepatitis C Virus RNA to Viral Core Antigen in Patient Sera. J Clin Microbiol 42:1977–1981.

50. Olofsson S-O, Bostrom K, Carlsson P, Boren J, Wettesten M, Bjursell G, Wikhmd O, Bondjers G. 1987. Structure and biosynthesis of apolipoprotein B. Apolipoprotein B 113:446–452.

51. Siwiak M, Zielenkiewicz P. 2013. Transimulation - Protein Biosynthesis Web Service. PLoS One 8.

52. Oh JW, Ito T, Lai MM. 1999. A recombinant hepatitis C virus RNA-dependent RNA polymerase capable of copying the full-length viral RNA. J Virol 73:7694–7702.

53. Ma H, Leveque V, De Witte A, Li W, Hendricks T, Clausen SM, Cammack N, Klumpp K. 2005. Inhibition of native hepatitis C virus replicase by nucleotide and non-nucleoside inhibitors. Virology 332:8–15.

54. Ingalls BP, Sauro HM. 2003. Sensitivity analysis of stoichiometric networks: An extension of metabolic control analysis to non-steady state trajectories. J Theor Biol 222:23–36.

Journal of Virology

JVI

Journal of Virology

Downloaded from http://jvi.asm.org/ on March 26, 2018 by LANL Research Library

Accepted Manuscript Posted Online

807 55. Martins J, Kroo IM, Alonso JJ. 2000. An automated method for sensitivity analysis using
808 complex variables. AIAA J.

809 56. 2017. SimBiology Documentation. MATLAB.

810 57. Chiș O, Banga JR, Balsa-Canto E. 2011. GenSSI : a software toolbox for structural
811 identifiability analysis of biological models 27:2610–2611.

812 58. Balsa-Canto E, Alonso AA, Banga JR. 2010. An iterative identification procedure for
813 dynamic modeling of biochemical networks. BMC Syst Biol 4.

814

815

Downloaded from http://jvi.asm.org/ on March 26, 2018 by LANL Research Library

Journal of Virology JVI Journal of Virology

Accepted Manuscript Posted Online

Journal of Virology

JVI

Journal of Virology

Downloaded from http://jvi.asm.org/ on March 26, 2018 by LANL Research Library

Figures

Figure 1 Schematic of the mathematical model of infectious HCV. (A) Diagram of the HCV polyprotein and its representation as various model species. (B) The entire model schematic and reactions involved. (1) A single initiator plus-stranded RNA associates with available ribosomes to form a translation complex, which then synthesizes the viral polyprotein. (2) The viral proteins are cleaved in a single step from the polyprotein, releasing a generalized structural protein and each of the non-structural proteins NS3/4A, NS5A, and NS5B. (3) RNA polymerase NS5B re-associates with a cytoplasmic RNA molecule, while NS5A associates with a host factor. Together these complexes are imported into the VMS in a second order reaction. (4) The minus strand of the viral RNA is synthesized from the newly imported plus-strand complex, after which it releases NS5B and forms a double-strand RNA molecule. (5) The dsRNA is bound once again by the NS5B molecule, which synthesizes new plus-strand RNA from this template. (6) VMS plus-strand RNA associates with a structural protein to assemble the viral particle, which is then exported into the extracellular environment.

Figure 2 Schematic comparison of two additional *cis*-acting protein mechanisms. The Binder/Clausznitzer mechanism has been proposed by previous modeling papers, and imports RNA into the VMS as part of an active translation complex in a third order reaction with NS5B and native host factor. An alternative cis-protein mechanism we propose assumes that the viral RNA stays associated with the polyprotein translated from it throughout the cleavage steps, whereas the final model (Figure 1) assumes it is free to release into the greater cytoplasmic RNA pool. This alternative model assumes the final RNA/NS5B complex can be imported to the VMS with the host factor complex, or be recycled at rate k_{TCR} for another round of translation.

Accepted Manuscript Posted Online

Journal of Virology

JVI

Journal of Virology

Downloaded from http://jvi.asm.org/ on March 26, 2018 by LANL Research Library

Figure 3 Acute HCVcc infection RNA and protein kinetic data. A 48-hour infection experiment using Huh7-1 cells with JFH-1 hepatitis C virus at an MOI of 3. (A) Profiles were calculated for the average total viral RNA (plus and minus-strand), core protein, and NS3 protein per cell over the course of the experiment, with the early time-points not used in fitting due to residual background levels of HCV RNA and core protein. (B) Extracellular titer data was calculated by counting foci-forming units (FFU) in the infection system throughout the 48-hour experiment. This was then converted to virions produced per cell using cell counts and previous data that showed 240 virions per FFU in an experiment with the same virus strain. (C) Western blot images for core, NS3, and actin proteins.

Figure 4 Viral protein degradation during early and late viral lifecycle. Western blot images for two 3-hour experiments beginning at 12 and 27 hours post-infection in the viral lifecycle. Infected cells were treated with cycloheximide at the respective time points to halt translation. The levels of core, NS3, and beta-actin were measured on hourly intervals afterwards by using a densitometry image analysis on the Western blot images and normalizing to actin level. Degradation rates at the 12- and 27-hour time points for core and NS3 were calculated based on the relative protein levels determined with the Western blot. In both cases the degradation rates were found to increase over the course of the infection experiment.

Figure 5 Comparison of three model variants for *cis*- and *trans*-acting protein behavior. (A) Fitted profiles for the mechanism used by previous models (Figure 2) for the involvement of *cis*-acting behavior of NS5B was proposed during model development and fit to the experimental

Accepted Manuscript Posted Online

Journal of Virology

JVI

Journal of Virology

Downloaded from http://jvi.asm.org/ on March 26, 2018 by LANL Research Library

data. This model requires that HCV RNA be imported into the VMS as part of an active translation complex (TC), along with NS5B and host factor (HF) in a third order reaction. The fitted profiles yielded an AIC of 530. (B) Fitted profiles for the alternative *cis*-protein mechanism proposed by this paper (Figure 2), which requires plus-stranded RNA to be imported into the VMS using only proteins translated from itself. This fit yielded an AIC of 983. (C) Fitted profiles for the final model's mechanism for both *cis*- and *trans*-acting behavior of NS5B, which is represented by association of the NS5B protein with cytoplasmic plus-strand RNA after its cleavage, and together the two are imported into the VMS. The fitted profiles yielded an AIC of 478.

Figure 6 VMS model structure comparison. The model was modified to represent the hypothesis that the VMS is segregated into independent vesicular replication complexes, such that the production rate of plus-strand RNA would depend only on the number of minus-strand RNA molecules present. The model yielded an AIC of 479, which is a comparable fit to that for the chosen final model in RNA fitting, with only minimal qualitative differences in the fitting observed.

Figure 7 Model fit with a constant core protein degradation rate. For comparison with our final model, the same model structure was refit to a new constant core protein degradation rate, as opposed to the changing core degradation rate that is part of the final model. This produced a slightly reduced fit quality.

Accepted Manuscript Posted Online

Journal of Virology

JVI

Journal of Virology

Downloaded from http://jvi.asm.org/ on March 26, 2018 by LANL Research Library

884 **Figure 8 Model validation.** The final model structure was validated by fitting to a separate set
885 of intracellular RNA data that was not involved in the original model development or parameter
886 determination. The new model fitting allowed the parameters corresponding to viral self-
887 interaction (k_{Rp5B}, k_{Rip}, $k_{assembly}$) to vary 10% in either direction.

888

889 **Figure 9 Sensitivity analysis for RNA, core, and NS3 relative to reaction constants.**
890 Sensitivities calculated for RNA, NS3, core protein (based on the surrogate structural protein),
891 and virions produced relative to reaction rates of our model. Similar patterns are observed across
892 each chart, with translation ($k_{translation}$), minus-strand synthesis ($k_{initiation}$), and replication
893 ($k_{replication}$) yielding the highest sensitivities. Virion production consistently showed the highest
894 sensitivity to model changes.

895

896 **Figure 10 Percent infected cells in MOI 3 experiment.** Cells were infected with an MOI of 3
897 for 3 hours before removal of the virus. At 24 hours post-inoculation the cells were fixed,
898 stained, and analyzed for percent infected, which was calculated by counting cells with viral
899 protein versus total cells. A blue Hoescht stain was used to stain DNA in all cells, and an anti-
900 NS5A antibody (red) was used to stain infected cells.

901

902 **Figure 11 Model structural identifiability tableaus.** Identifiability analysis was conducted for
903 the eight parameters that did not have a literature or experimental basis in our model: k_{TC},
904 $k_{translation}$, $k_{cleavage}$, k_{HFC}, k_{Rp5B}, k_{Rip}, $k_{assembly}$, *and* k_{degRp}. Our analysis used iterative Lie derivatives
905 to calculate successive identifiability tableaus, i.e. Jacobian matrices, as described previously by

Accepted Manuscript Posted Online

Journal of Virology

JVI

Journal of Virology

Downloaded from http://jvi.asm.org/ on March 26, 2018 by LANL Research Library

Chiş et al. and Balsa-Canto et al. (57, 58). Non-zero elements, marked by filled in black spaces in the grid, indicate that the Lie derivative component (a coefficient of a power series representative of the system) depends on that parameter. Blank columns indicate non-identifiability. The reduced tableau demonstrates identifiable parameters and can be used to create a system of equations for identifying parameters.

Accepted Manuscript Posted Online

Journal of Virology

JVI

Journal of Virology

Downloaded from http://jvi.asm.org/ on March 26, 2018 by LANL Research Library

911 **Tables**

912 **Table 1** Model parameter estimates obtained from experiment, literature and simulation.

	Parameter Estimate	Description	Source
Translation			
k_{TC}	1 molecule^{-1} hour^{-1}	Transcription complex formation	(8)
$k_{translation}$	180 hour^{-1}	Polyprotein translation rate	Fitting
$k_{cleavage}$	9 hour^{-1}	Structural protein cleavage rate	Fitting
Replication			
k_{HFC}	0.0008 molecule^{-1} hour^{-1}	Host factor/NS5A complex formation	Fitting
k_{Rp5B}	0.1 molecule^{-1} hour^{-1}	(+)RNA/NS5B complex formation	Fitting
k_{Rip}	0.6 molecule^{-1} hour^{-1}	(+)RNA and NS5B import into VMS	Fitting
$k_{initiation}$	1.12 hour^{-1}	(-)RNA synthesis	(6, 52, 53)
k_{Rids}	10 molecule^{-1} hour^{-1}	dsRNA replication complex formation	(8)
$k_{replication}$	1.12 hour^{-1}	(+)RNA synthesis	(6, 52, 53)
Import/Export			
k_{outRp}	0.307 hour^{-1}	(+)RNA transport from VMS to cytoplasm	(8)
$k_{assembly}$	6.7×10^{-10} molecule^{-1} hour^{-1}	Viral particle assembly	Fitting
Degradation			
k_{degRp}	0.26 hour^{-1}	Cytoplasmic (+)RNA degradation	Fitting
k_{degS}	Initial: 0.61 h^{-1} Final: 0.10 h^{-1}	Structural protein degradation	Experimental data
k_{degNS}	0.11 hour^{-1}	NS3/4A degradation	Experimental data
k_{degVMS}	0.001 hour^{-1}	VMS species degradation	Fitting, (38, 39)

Accepted Manuscript Posted Online

Journal of Virology

JVI

Journal of Virology

Host Species		
Ribosomes	5000 molecules	Fitting
Host Factor	30 molecules	Fitting
Initial Values		
Plus-stranded RNA	1 molecule	
Core protein	180 molecules	

913

914

Downloaded from http://jvi.asm.org/ on March 26, 2018 by LANL Research Library

Accepted Manuscript Posted Online

Journal of Virology

JVI

Journal of Virology

Downloaded from http://jvi.asm.org/ on March 26, 2018 by LANL Research Library

915 **Table 2:** Ordinary differential equations for the final model

Species		Equation
	Cytoplasm	
Plus-strand RNA	$\frac{d[R_p^{cyt}]}{dt} = -k_{Tc}[Ribo][R_p^{cyt}] + k_{trans}[TC] - k_{Rp5B}[R_p^{cyt}][NS5B] + k_{outRp}[R_p^{VMS}] - k_{degRp}[R_p^{cyt}]$	1
Ribosomes	$\frac{d[Ribo]}{dt} = -k_{Tc}[Ribo][R_p^{cyt}] + k_{trans}[TC]$	2
Translation complex	$\frac{d[TC]}{dt} = k_{Tc}[Ribo][R_p^{cyt}] - k_{trans}[TC]$	3
Polyprotein	$\frac{d[PP]}{dt} = k_{trans}[TC] - k_{Ckeavage}[PP]$	4
Core protein	$\frac{d[S]}{dt} = k_S[PP] - k_{degS}\,[S] - 180\,k_{Assembly}[R_p^{VMS}][S]$	5
NS3/4A protein complex	$\frac{d[NS34A]}{dt} = k_{Cleavage}[PP] - k_{degNS}\,[NS34A]$	6
NS5A protein	$\frac{d[NS5A]}{dt} = k_{Cleavage}[PP] - k_{degNS}\,[NS5A] - k_{HFC}[NS5A][HF]$	7
Cytoplasmic NS5B protein	$\frac{d[NS5B^{cyt}]}{dt} = k_{Cleavage}[PP] - k_{degNS}\,[NS5B^{cyt}] - k_{Rp5B}[R_p^{cyt}][NS5B^{cyt}]$	8
Host factor	$\frac{d[HF]}{dt} = -k_{HFC}[HF][NS5A] + k_{init}[R_{ip}]$	9
NS5A/host factor complex	$\frac{d[HFC]}{dt} = k_{HFC}[HF][NS5A] - k_{Rip}[Rp5B][HFC]$	10
RNA/NS5B complex	$\frac{d[Rp5B]}{dt} = k_{Rp5B}[R_p^{cyt}][NS5B^{cyt}] - k_{Rip}[Rp5B][HFC]$	11
	VMS	
Plus-strand RNA complex	$\frac{d[R_{ip}]}{dt} = k_{Rip}[Rp5B][HFC] - k_{init}[R_{ip}] - k_{degVMS}[R_{ip}]$	12

Accepted Manuscript Posted Online

Double-strand RNA	$\frac{d[dsRNA]}{dt} = k_{init}[R_{ip}] - k_{Rids}[dsRNA][NS5B^{VMS}] - k_{degVMS}[dsRNA] + k_{repl}[R_{ids}]$	13
VMS NS5B	$\frac{d[NS5B^{VMS}]}{dt} = k_{init}[R_{ip}] - k_{Rids}[dsRNA][NS5B^{VMS}] - k_{degVMS}[NS5B^{VMS}] + k_{repl}[R_{ids}]$	14
dsRNA complex	$\frac{d[R_{ids}]}{dt} = k_{Rids}[dsRNA][NS5B^{VMS}] - k_{repl}[R_{ids}] - k_{degVMS}[Rids]$	15
VMS plus-strand RNA	$\frac{d[R_p^{VMS}]}{dt} = k_{repl}[R_{ids}] - k_{Assembly}[S][R_p^{VMS}] - k_{degVMS}[R_p^{VMS}] - k_{outRp}[R_p^{VMS}]$	16
Extracellular Environment		
Secreted viral particle	$\frac{d[V_{created}]}{dt} = k_{Assembly}[S][R_p^{VMS}]$	17

916

917

Journal of Virology

JVI

Journal of Virology

Downloaded from http://jvi.asm.org/ on March 26, 2018 by LANL Research Library

Accepted Manuscript Posted Online

Journal of Virology

JVI

Journal of Virology

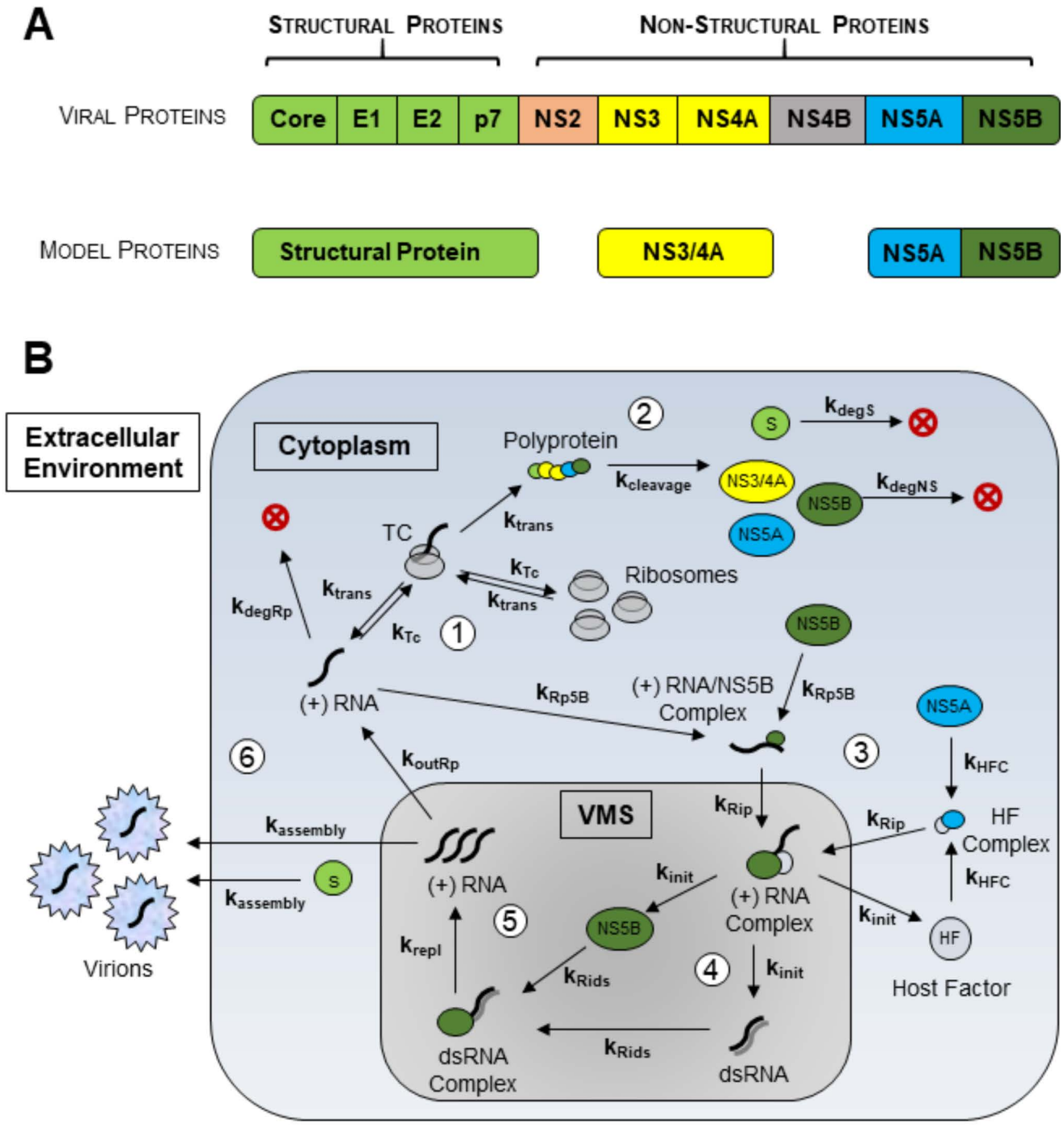

Downloaded from http://jvi.asm.org/ on March 26, 2018 by LANL Research Library

Accepted Manuscript Posted Online

Journal of Virology

JVI

Journal of Virology

Downloaded from http://jvi.asm.org/ on March 26, 2018 by LANL Research Library

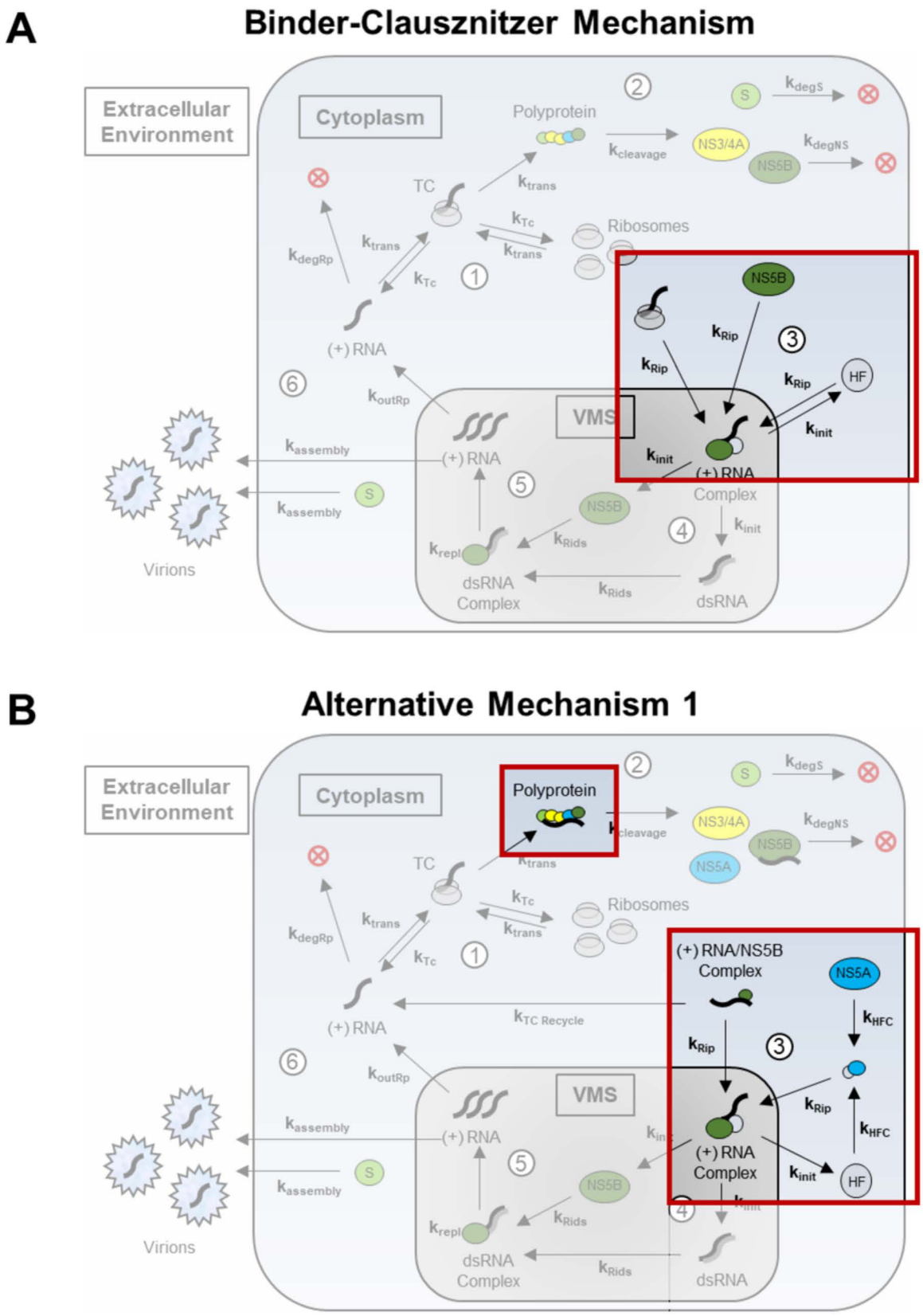

Accepted Manuscript Posted Online

Journal of Virology

JVI

Journal of Virology

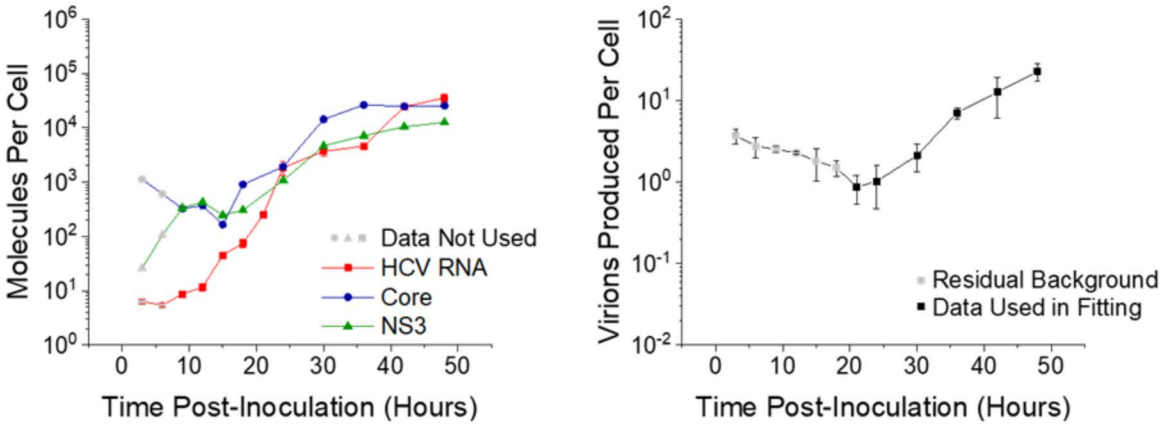

Downloaded from http://jvi.asm.org/ on March 26, 2018 by LANL Research Library

Accepted Manuscript Posted Online

Journal of Virology

JVI

Journal of Virology

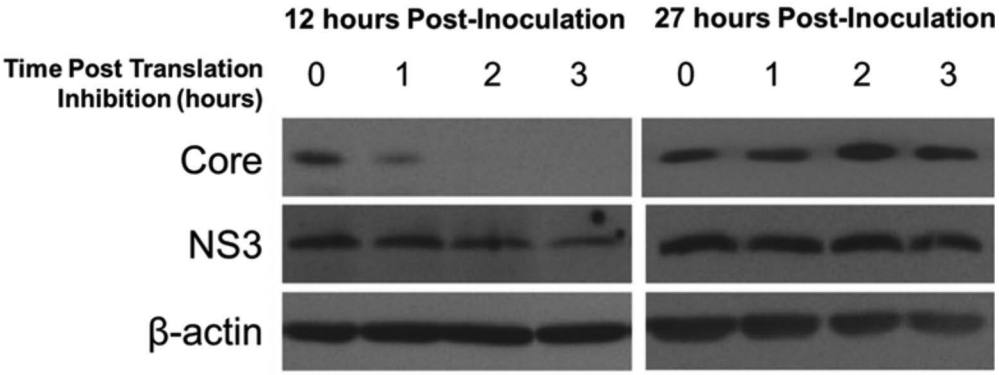

	Core Degradation Rate	NS3 Degradation Rate
12 hours Post-Infection	0.61 h^{-1}	0.11 h^{-1}
27 hours Post-Infection	0.10 h^{-1}	0.05 h^{-1}

Downloaded from http://jvi.asm.org/ on March 26, 2018 by LANL Research Library

Accepted Manuscript Posted Online

Journal of Virology

JVI

Journal of Virology

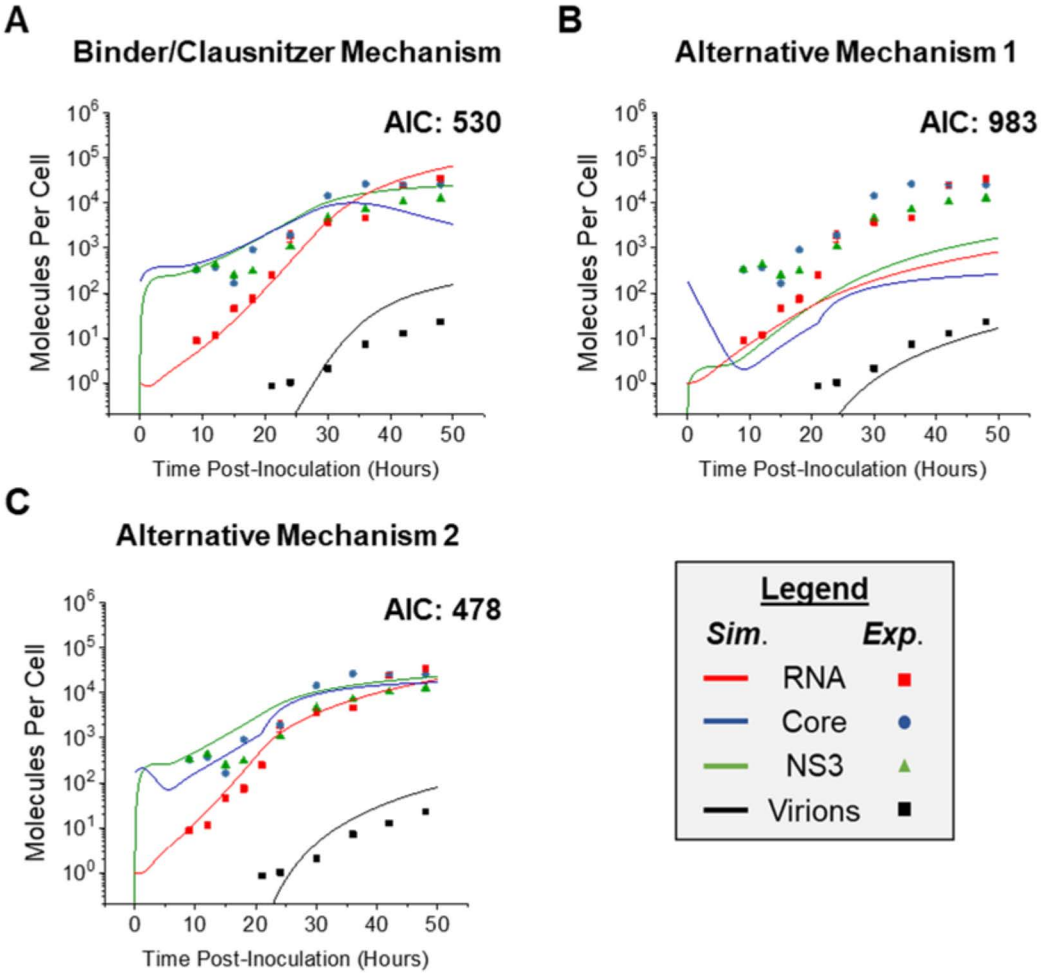

Downloaded from http://jvi.asm.org/ on March 26, 2018 by LANL Research Library

Accepted Manuscript Posted Online

Journal of Virology

JVI

Journal of Virology

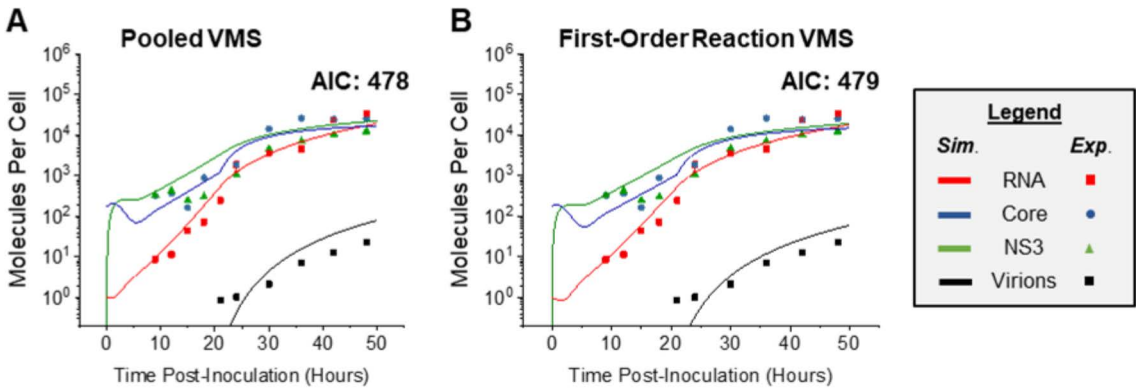

Downloaded from http://jvi.asm.org/ on March 26, 2018 by LANL Research Library

Accepted Manuscript Posted Online

Journal of Virology

JVI

Journal of Virology

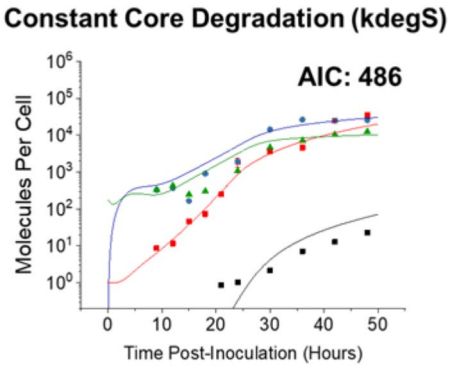

Downloaded from http://jvi.asm.org/ on March 26, 2018 by LANL Research Library

Accepted Manuscript Posted Online

Journal of Virology

JVI

Journal of Virology

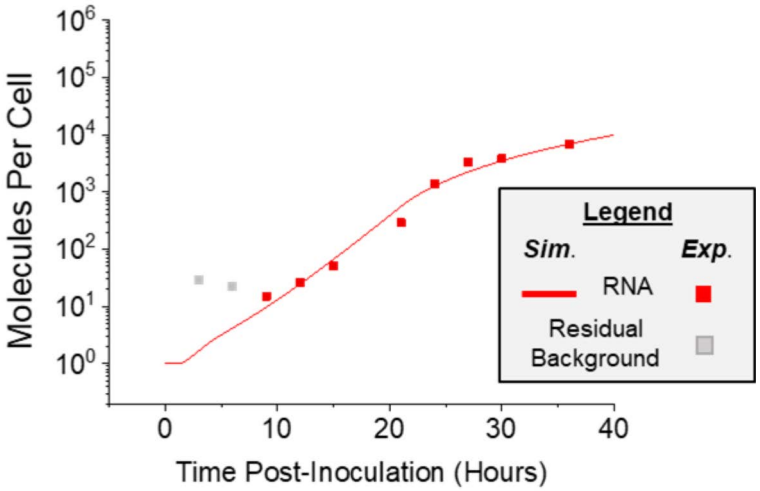

Parameter	Training Value (molecule^{-1} h^{-1})	Validation Value (molecule^{-1} h^{-1})
k_{Rp5B}	0.1	0.0103
k_{Rip}	0.6	0.66
$k_{Assembly}$	1.2×10^{-7}	1.1×10^{-7}

Downloaded from http://jvi.asm.org/ on March 26, 2018 by LANL Research Library

Accepted Manuscript Posted Online

Journal of Virology

JVI

Journal of Virology

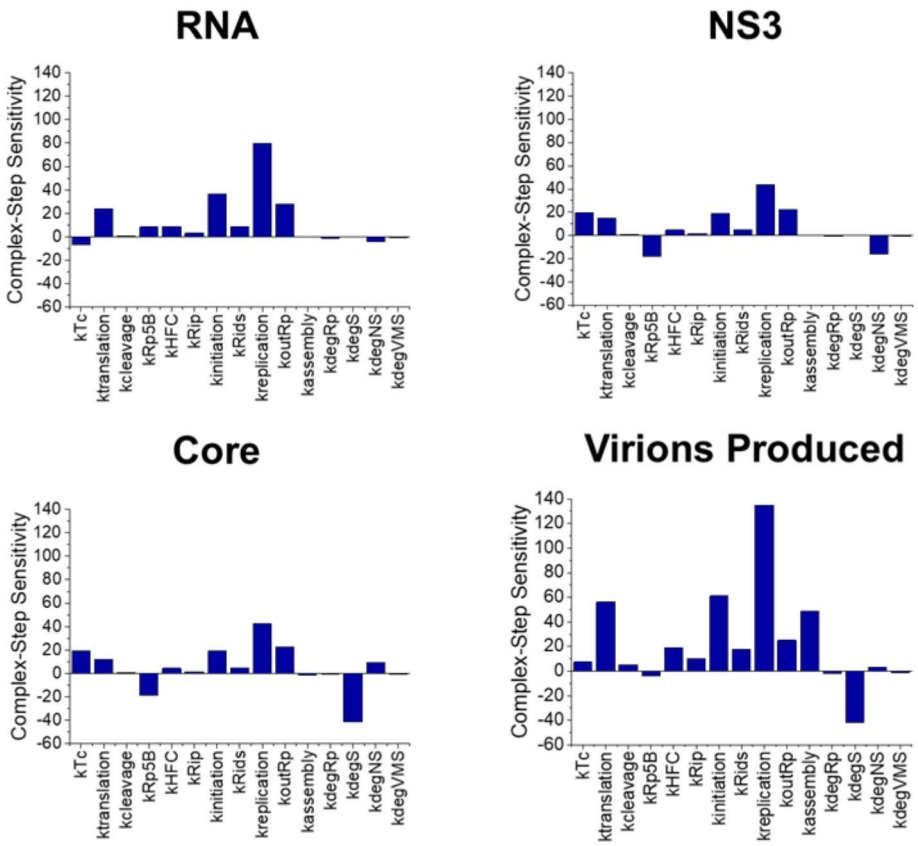

Downloaded from http://jvi.asm.org/ on March 26, 2018 by LANL Research Library

Accepted Manuscript Posted Online

Journal of Virology

JVI

Journal of Virology

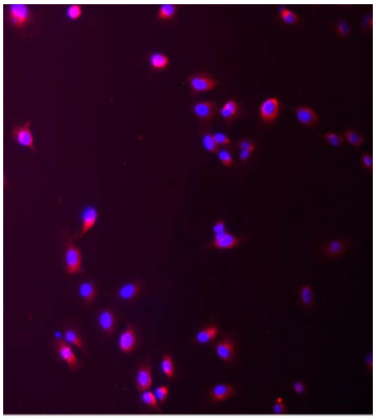

Infected cells:	121
Total cells:	127
% Infected:	95.28%

Downloaded from http://jvi.asm.org/ on March 26, 2018 by LANL Research Library

Accepted Manuscript Posted Online

Journal of Virology

JVI

Journal of Virology

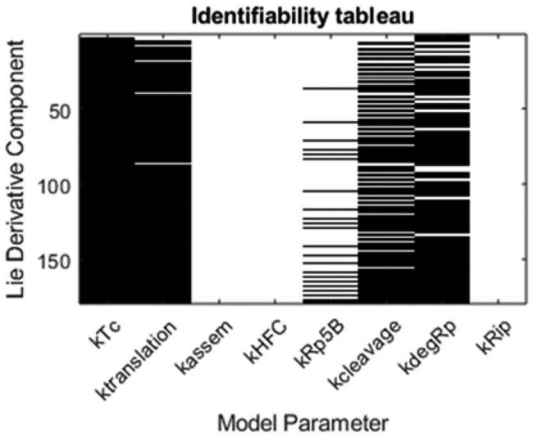

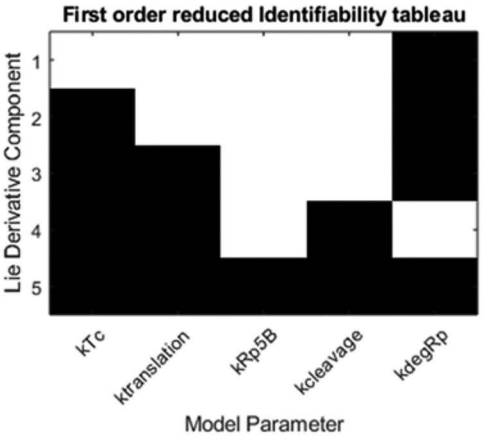

Downloaded from http://jvi.asm.org/ on March 26, 2018 by LANL Research Library